

# *Advances in the subseasonal prediction of extreme events: relevant case studies across the globe*

Article

Accepted Version

Domeisen, D. I.V., White, C. J., Afargan-Gerstman, H., Munoz, A. G., Jaiga, M. A., Vitart, F., Wulff, C. O., Antoine, S., Ardilouze, C., Batte, L., Bloomfield, H. C. ORCID: <https://orcid.org/0000-0002-5616-1503>, Brayshaw, D. J. ORCID: <https://orcid.org/0000-0002-3927-4362>, Camargo, S. J., Charlton-Perez, A. ORCID: <https://orcid.org/0000-0001-8179-6220>, Collins, D., Cowan, T., del Mar Chaves, M., Ferranti, L., Gomez, R., Gonzalez, P. L. M. ORCID: <https://orcid.org/0000-0003-0154-0087>, Gonzalez Romero, C., Infant, J. M., Karozis, S., Kim, H., Kolstad, E. W., LaJoie, E., Lledo, L., Magnusson, L., Malguzzi, P., Manrique-Sunen, A., Mastrangelo, D., Materia, S., Medina, H., Palma, L., Pineda, L. E., Sfetsos, A., Son, S.-W., Soret, A., Strazzo, S. and Tian, D. (2022) Advances in the subseasonal prediction of extreme events: relevant case studies across the globe. *Bulletin of the American Meteorological Society*, 103 (6). pp. 1473-1501. ISSN 1520-0477 doi: 10.1175/BAMS-D-20-0221.1 Available at <https://centaur.reading.ac.uk/104243/>

work. See [Guidance on citing](#).

To link to this article DOI: <http://dx.doi.org/10.1175/BAMS-D-20-0221.1>

Publisher: American Meteorological Society

All outputs in CentAUR are protected by Intellectual Property Rights law, including copyright law. Copyright and IPR is retained by the creators or other copyright holders. Terms and conditions for use of this material are defined in the [End User Agreement](#).

[www.reading.ac.uk/centaur](http://www.reading.ac.uk/centaur)

**CentAUR**

Central Archive at the University of Reading

Reading's research outputs online

# 1 **Advances in the subseasonal prediction of extreme events:**

## 2 **Relevant case studies across the globe**

3 Daniela I.V. Domeisen \*

4 Christopher J. White

5 *Department of Civil and Environmental Engineering, University of Strathclyde, Glasgow, UK*

6 Hilla Afargan-Gerstman

7 *ETH Zurich, Institute for Atmospheric and Climate Science, Zurich, Switzerland*

8 Ángel G. Muñoz

9 *International Research Institute for Climate and Society (IRI), Columbia University's Climate*

10 *School, and The Earth Institute at Columbia University, New York, U.S.A*

11 Matthew A. Janiga

12 *Naval Research Laboratory, Monterey CA, U.S.A*

13 Frédéric Vitart

14 *European Centre for Medium-Range Weather Forecasts, Reading, UK*

15 C. Ole Wulff

16 *ETH Zurich, Institute for Atmospheric and Climate Science, Zurich, Switzerland / NORCE*

17 *Norwegian Research Centre, Bjerknes Centre for Climate Research, Bergen, Norway*

18

Salomé Antoine

19

*CNRM, Université de Toulouse, Météo-France, CNRS, Toulouse, France*

20

Constantin Ardilouze

21

*CNRM, Université de Toulouse, Météo-France, CNRS, Toulouse, France*

22

Lauriane Batté

23

*CNRM, Université de Toulouse, Météo-France, CNRS, Toulouse, France*

24

Hannah C. Bloomfield

25

*Department of Meteorology, University of Reading, UK / School of Geographical Sciences,*

26

*University of Bristol, UK*

27

David J. Brayshaw

28

*Department of Meteorology, University of Reading, UK*

29

Suzana J. Camargo

30

*Lamont-Doherty Earth Observatory, Columbia University, Palisades, NY, U.S.A*

31

Andrew Charlton-Pérez

32

*Department of Meteorology, University of Reading, UK*

33

Dan Collins

34

*Climate Prediction Center, NOAA/NWS/NCEP, College Park, MD, U.S.A*

35

Tim Cowan

<sup>36</sup> *Centre for Applied Climate Sciences, University of Southern Queensland, Toowoomba, Australia /*  
<sup>37</sup> *Bureau of Meteorology, Melbourne, Australia*

<sup>38</sup> **Maria del Mar Chaves**

<sup>39</sup> *Climate Simulations and Predictions, Centro Euro-Mediterraneo sui Cambiamenti Climatici,*  
<sup>40</sup> *Bologna, Italy / now at: University of Bologna, Bologna, Italy*

<sup>41</sup> **Laura Ferranti**

<sup>42</sup> *European Centre for Medium-Range Weather Forecasts, Reading, UK*

<sup>43</sup> **Rosario Gómez**

<sup>44</sup> *Organismo Internacional Regional de Sanidad Agropecuaria, San Salvador, El Salvador*

<sup>45</sup> **Paula L.M. González**

<sup>46</sup> *NCAS/Department of Meteorology, University of Reading, UK / International Research Institute  
47 for Climate and Society, The Earth Institute, Columbia University, U.S.A*

<sup>48</sup> **Carmen González Romero**

<sup>49</sup> *International Research Institute for Climate and Society (IRI). Columbia University's Climate  
50 School, and The Earth Institute at Columbia University. New York, U.S.A*

<sup>51</sup> **Johnna M. Infantí**

<sup>52</sup> *Climate Prediction Center, NOAA/NWS/NCEP, College Park, MD, U.S.A*

<sup>53</sup> **Stelios Karozis**

<sup>54</sup> *National Centre for Scientific Research "Demokritos", Greece*

55

Hera Kim

56

*School of Earth and Environmental Sciences, Seoul National University, South Korea*

57

Erik W. Kolstad

58

*NORCE Norwegian Research Center, Bjerknes Center for Climate Research, Bergen, Norway*

59

Emerson LaJoie

60

*Climate Prediction Center, NOAA/NWS/NCEP, College Park, MD, U.S.A*

61

Llorenç Lledó

62

*Barcelona Supercomputing Center (BSC), Barcelona, Spain*

63

Linus Magnusson

64

*European Centre for Medium-Range Weather Forecasts, Reading, UK*

65

Piero Malguzzi

66

*CNR-ISAC, Bologna, Italy*

67

Andrea Manrique-Suñén

68

*Barcelona Supercomputing Center (BSC), Barcelona, Spain*

69

Daniele Mastrangelo

70

*CNR-ISAC, Bologna, Italy*

71

Stefano Materia

72

*Climate Simulations and Predictions, Centro Euro-Mediterraneo sui Cambiamenti Climatici,*

73

*Bologna, Italy*

74

Hanoi Medina

75     *Department of Crop, Soil, and Environmental Sciences, Auburn University, Auburn, AL, U.S.A*

76

Lluís Palma

77     *Barcelona Supercomputing Center (BSC), Barcelona, Spain*

78

Luis E. Pineda

79     *Yachay Tech University, School of Earth Sciences, Energy and Environment, Hda. San José s/n y*

80     *Proyecto Yachay, Urcuquí, Ecuador*

81

Athanasios Sfetsos

82     *National Centre for Scientific Research "Demokritos", Greece*

83

Seok-Woo Son

84     *School of Earth and Environmental Sciences, Seoul National University, South Korea*

85

Albert Soret

86     *Barcelona Supercomputing Center (BSC), Barcelona, Spain*

87

Sarah Strazzo

88     *Embry Riddle Aeronautical University, Daytona Beach, FL, U.S.A*

89

Di Tian

90     *Department of Crop, Soil, and Environmental Sciences, Auburn University, Auburn, AL, U.S.A*

91     \*Corresponding author: Daniela I.V. Domeisen, daniela.domeisen@env.ethz.ch

## ABSTRACT

92 Extreme weather events have devastating impacts on human health, economic activities, ecosystems, and infrastructure. It is therefore crucial to anticipate extremes and their impacts to allow  
93 for preparedness and emergency measures. There is indeed potential for probabilistic subseasonal  
94 prediction on timescales of several weeks for many extreme events. Here we provide an overview  
95 of subseasonal predictability for case studies of some of the most prominent extreme events across  
96 the globe using the ECMWF S2S prediction system: heatwaves, cold spells, heavy precipitation  
97 events, and tropical and extratropical cyclones. The considered heatwaves exhibit predictability on  
98 timescales of 3-4 weeks, while this timescale is 2-3 weeks for cold spells. Precipitation extremes  
99 are the least predictable among the considered case studies. Tropical cyclones, on the other hand,  
100 can exhibit probabilistic predictability on timescales of up to 3 weeks, which in the presented cases  
101 was aided by remote precursors such as the Madden-Julian Oscillation. For extratropical cyclones,  
102 lead times are found to be shorter. These case studies clearly illustrate the potential for event -  
103 dependent advance warnings for a wide range of extreme events. The subseasonal predictability of  
104 extreme events demonstrated here allows for an extension of warning horizons, provides advance  
105 information to impact modelers, and informs communities and stakeholders affected by the impacts  
106 of extreme weather events.  
107

<sup>108</sup> *Capsule summary.* An assessment and comparison of the subseasonal predictability of case  
<sup>109</sup> studies of the most prominent extreme weather events on a global scale: heatwaves, cold spells,  
<sup>110</sup> precipitation extremes, and cyclones.

<sup>111</sup>

## <sup>112</sup> **1. Subseasonal prediction of extreme events**

<sup>113</sup> Extreme weather events pose threats to humans, infrastructure, and ecosystems. In a changing  
<sup>114</sup> climate, many extremes are projected to increase in strength, frequency, and/or duration, and it is  
<sup>115</sup> therefore increasingly important to anticipate extreme events and their impacts as early as possible.

<sup>116</sup> A successful prediction several weeks in advance will benefit stakeholders' decision making for  
<sup>117</sup> emergency management (White et al. 2017; Merz et al. 2020; White et al. 2021). Indeed, there  
<sup>118</sup> is increasing potential for probabilistic subseasonal prediction on timescales of several weeks  
<sup>119</sup> for extreme events (Vitart 2014; Vitart and Robertson 2018; Robertson et al. 2020). Increased  
<sup>120</sup> predictability can arise from remote drivers or long-lived precursor patterns that are conducive to  
<sup>121</sup> the occurrence of extreme events. These drivers include tropical precursors such as the Madden-  
<sup>122</sup> Julian Oscillation (MJO) (e.g. Vitart and Molteni 2010; Rodney et al. 2013) and El Niño Southern  
<sup>123</sup> Oscillation (ENSO) (e.g. Domeisen et al. 2015), surface interactions with snow cover (e.g. Cohen  
<sup>124</sup> and Jones 2011) or sea ice (e.g. Sun et al. 2015), the upper atmosphere (e.g. Domeisen et al. 2020b;  
<sup>125</sup> Domeisen and Butler 2020), or a combination of predictors (Muñoz et al. 2015, 2016; Doss-Gollin  
<sup>126</sup> et al. 2018; Dobrynin et al. 2018). A better understanding of these precursors can contribute to  
<sup>127</sup> increased predictability. At the same time, improvements in the prediction of extremes arises from  
<sup>128</sup> progress in the performance of prediction systems through advancements in process representation,  
<sup>129</sup> coupling, and parameterization, as well as model resolution (Bauer et al. 2015). Merryfield et al.  
<sup>130</sup> (2020) recommended an assessment of the predictability of historical high-impact weather events

131 as a way forward to demonstrate the potential benefits of subseasonal to seasonal (S2S) forecasts.  
132 Here we discuss extreme event predictability based on a state-of-the-art subseasonal prediction  
133 system and a range of precursors for selected case studies of high-impact extremes in Europe,  
134 Africa, Asia, Australia, as well as South, Central, and North America for the most prominent  
135 extreme events on a global scale: heatwaves, cold spells, heavy precipitation events, and both  
136 tropical and extratropical cyclones. The following sections provide a brief overview of the physical  
137 drivers and potential for predictability for these extreme events, while the subsequent sections dive  
138 into the specific case studies.

139 *a. Heatwaves*

140 Heatwaves over land have devastating impacts on human health and ecosystems (Campbell et al.  
141 2018; Yang et al. 2019), agriculture (Brás et al. 2021), and energy demand (Auffhammer et al.  
142 2017; Bloomfield et al. 2020). Over the past decades, heatwaves have significantly increased  
143 in frequency and intensity (Perkins et al. 2012) with further increases predicted for the future  
144 (Watanabe et al. 2013; Lopez et al. 2018), largely due to anthropogenic global warming (Stocker  
145 2014; Shiogama et al. 2014). Heatwaves are commonly characterized by temperature and duration  
146 thresholds (Russó et al. 2014), in addition to humidity and diurnal temperature cycle characteristics  
147 for applications to human morbidity and mortality (e.g. Raymond et al. 2020).

148 Heatwaves are often associated with persistent anticyclonic circulation patterns (Li et al. 2015;  
149 Freychet et al. 2017) that can sometimes be identified as blocking (Pfahl and Wernli 2012; Schaller  
150 et al. 2018; Brunner et al. 2018; Carrera et al. 2004; Dong et al. 2018; Li et al. 2019; Yeo et al.  
151 2019), long-lived Rossby Wave Packets (RWPs, Wirth et al. (2018)), which can contribute to  
152 predictability (Fragkoulidis et al. 2018; Grazzini and Vitart 2015), or quasi-stationary wave trains  
153 (Enomoto 2004; Kim et al. 2018; Li et al. 2019). These patterns can be triggered or enhanced

154 by remote effects. For instance, sea surface temperature (SST) anomalies in subtropical and  
155 extratropical ocean basins can help induce European and North American heatwaves (Wulff et al.  
156 2017; Duchezi et al. 2016; McKinnon et al. 2016; Hartmann 2015), and East Asian heatwaves can  
157 be triggered by the North Atlantic Oscillation (NAO), Ural blocking, and diabatic heating in the  
158 eastern Mediterranean (Yasui and Watanabe 2010; Jian-Qi 2012; Wu et al. 2016; Gao et al. 2018;  
159 Li et al. 2019).

160 These remote forcings can enhance the predictability of heatwaves. Recent research has in-  
161 deed shown potential for the extended-range prediction of heatwaves on sub-seasonal to seasonal  
162 timescales (Kueh and Lin 2020; Koster et al. 2010; Luo and Zhang 2012; Pepler et al. 2015; Tian  
163 et al. 2017; Wulff and Domeisen 2019). In addition, heatwaves can also be exacerbated by land-  
164 atmosphere feedbacks (e.g. Fischer et al. 2007; Mueller and Seneviratne 2012; Miralles et al. 2014;  
165 Hauser et al. 2016; Seneviratne et al. 2010; Berg and Sheffield 2018; Tian et al. 2016, 2018) and  
166 improvements in soil moisture initialization can therefore increase the predictability of heatwaves  
167 (Ferranti and Viterbo 2006; Dirmeyer et al. 2018; Bunzel et al. 2018).

168 *b. Cold spells*

169 Cold spells can affect electricity production (Beerli et al. 2017; Gruber et al. 2021; Doss-Gollin  
170 et al. 2021) and demand (Cradden and McDermott 2018; Bloomfield et al. 2018, 2020), human  
171 mortality (Charlton-Perez et al. 2019, 2021), and agriculture (Materia et al. 2020a). Similar to  
172 heatwaves, cold spells are often defined by temperature and duration thresholds (de Vries et al.  
173 2012). Like heatwaves, cold spells can be related to atmospheric blocking and hence model  
174 biases in blocking frequency can impair predictions at lead times beyond two weeks (Hamill  
175 and Kiladis 2014; Quinting and Vitart 2019). Predictability can be gained from tropical drivers  
176 such as the MJO, and model performance can be enhanced by capturing the predictable signal of

<sup>177</sup> large-scale weather patterns such as the NAO at the extended range (Ferranti et al. 2018). Blocking  
<sup>178</sup> associated with the negative phase of the NAO can also be induced through sudden stratospheric  
<sup>179</sup> warming (SSW) events (Thompson et al. 2002; Lehtonen and Karpechko 2016; Charlton-Perez  
<sup>180</sup> et al. 2018; Domeisen 2019), which can induce cold spells both over land (Kolstad et al. 2010)  
<sup>181</sup> and ocean (Afargan-Gerstman et al. 2020). However, not all regions gain predictability skill from  
<sup>182</sup> stratospheric forcing (Domeisen et al. 2020b; Materia et al. 2020a).

<sup>183</sup>

#### <sup>184</sup> *c. Precipitation events*

<sup>185</sup> Heavy precipitation events can lead to flooding as well as land- or mudslides, and they are often  
<sup>186</sup> accompanied by strong winds and low temperatures, the combination of which can be detrimental  
<sup>187</sup> to humans, agriculture and infrastructure (Zscheischler et al. 2020). Heavy precipitation events are  
<sup>188</sup> projected to become more frequent in many regions (Donat et al. 2016; Prein et al. 2017) due to  
<sup>189</sup> anthropogenic climate change (Westra et al. 2013; Zhang et al. 2013; Li, Chao et al. 2021). Similar  
<sup>190</sup> to temperature extremes, rainfall extremes arise through persistent atmospheric conditions, which  
<sup>191</sup> can be triggered or maintained by large-scale forcing (e.g. from ENSO and the MJO (Jones et al.  
<sup>192</sup> 2004; Kenyon and Hegerl 2010; Muñoz et al. 2015)), atmospheric blocking (Lenggenhager and  
<sup>193</sup> Martius 2019), or monsoon systems (Zhang and Zhou 2019).

<sup>194</sup> Precipitation extremes tend to be less predictable than temperature extremes such as warm and  
<sup>195</sup> cold spells (de Andrade et al. 2019). The ability of a prediction system to predict rainfall extremes  
<sup>196</sup> beyond deterministic timescales is related to the simulation of the connection between precipitation  
<sup>197</sup> and its large-scale forcing such as ENSO and the MJO (Vigaud et al. 2017; Specq et al. 2020)  
<sup>198</sup> or atmospheric rivers (DeFlorio et al. 2019). Regions with strong ENSO teleconnections exhibit  
<sup>199</sup> better predictability of rainfall extremes, as for example, in Australia (King et al. 2020) or the

200 southwestern U.S. (Gershunov 1998; Pan et al. 2019), if ENSO is correctly simulated (Bayr et al.  
201 2019). Interference of drivers on multiple timescales can further modulate the intensity, occurrence  
202 and predictability of precipitation extremes (Muñoz et al. 2015, 2016).

203 *d. Tropical Cyclones and Medicanes*

204 Tropical and extratropical cyclones impact human lives and livelihoods and lead to large envi-  
205 ronmental impacts and economic losses (Camargo and Hsiang 2015; Hsiang 2010; Hsiang and  
206 Narita 2012). Anthropogenic climate change affects various properties of tropical cyclones (TC),  
207 in particular their intensity, as well as the precipitation and storm surge associated with these  
208 events (Knutson et al. 2019, 2020). While individual cyclones' genesis, tracks and intensity are  
209 not predictable beyond deterministic timescales, large-scale drivers can provide predictability in a  
210 probabilistic sense on S2S timescales. On seasonal timescales, ENSO modifies the characteristics  
211 of TC frequency, intensity and tracks (e.g., Vitart et al. 2003; Lin et al. 2017; Nicholls 1979; Evans  
212 and Allan 1992). On subseasonal timescales, TC activity is enhanced (decreased) during and after  
213 an active (suppressed) MJO (e.g. Camargo et al. 2019), especially in the southern hemisphere  
214 (e.g. Hall et al. 2001; Camargo et al. 2009), allowing for successful statistical forecasts (Leroy and  
215 Wheeler 2008). Recently, the performance of dynamical models for forecasting TCs on subsea-  
216 sonal timescales has significantly improved (Camp et al. 2018; Camargo et al. 2019; Robertson  
217 et al. 2020; Vitart et al. 2010; Camargo et al. 2021). A successful example is cyclone Hilda, which  
218 made landfall in northwestern Australia and was predicted 3 weeks in advance (Gregory et al.  
219 2019). However, this success is not consistent across models, and is likely linked to a successful  
220 prediction of the MJO (Vitart 2017; Lee et al. 2018, 2020).

221 In addition to tropical cyclones, we also consider *medicanes* ("Mediterranean Hurricanes"), rare  
222 intense and high-impact extratropical cyclones in the Mediterranean region (Ulbrich et al. 2009;

<sup>223</sup> Cavicchia et al. 2014; Mylonas et al. 2018; Flaounas et al. 2021). These events occur on average  
<sup>224</sup> 1.6 times / year (Flaounas et al. 2015) and can lead to severe damage in coastal areas associated  
<sup>225</sup> with flooding and high winds.

<sup>226</sup> **2. Data and Methods**

<sup>227</sup> To evaluate the subseasonal prediction of the above extreme events we use both forecasts and  
<sup>228</sup> hindcasts (historical forecasts) from the extended-range operational ensemble prediction system  
<sup>229</sup> (Vitart et al. 2008) from the European Centre for Medium-Range Weather Forecasts (ECMWF),  
<sup>230</sup> which is part of the S2S database (Vitart et al. 2017). The prediction system includes coupling  
<sup>231</sup> with the ocean and sea ice (Buizza et al. 2017). The atmospheric model has a horizontal resolution  
<sup>232</sup> of approximately 36 km and 91 vertical levels with a model lid at 0.01 hPa (at the time of data  
<sup>233</sup> download for this study). Where available, that is, for case studies after June 2015, forecasts from  
<sup>234</sup> the prevailing model version were used (cycles 43R1, 43R3 and 45R1); these ensemble forecasts  
<sup>235</sup> consist of 51 members. For the case studies using hindcasts, the 11-member hindcast ensemble  
<sup>236</sup> from model cycle 46R1 was used. Both forecasts and hindcasts are initialized twice weekly.

<sup>237</sup> The target weeks are selected for each case study individually based on the week of the most  
<sup>238</sup> extreme anomalies. Since the forecasts are only initialized twice weekly, it is not always possible  
<sup>239</sup> to find a forecast that is initialized exactly the day before week 1. Week-1 lead time for a specific  
<sup>240</sup> case study is therefore chosen such that the target week lies directly on or after the initialization,  
<sup>241</sup> that is, the forecast is initialized either on the first day of week 1 or up to two days earlier. The  
<sup>242</sup> additional forecast lead weeks (weeks 2 - 4) then lie exactly adjacent to week 1.

<sup>243</sup> To compute anomalies for the subseasonal predictions, a 7-day mean climatology is computed  
<sup>244</sup> based on the 11-member ensemble hindcasts initialized for the same lead time for the corresponding  
<sup>245</sup> available 20-year hindcast period. For example, for the California heatwave on 23 July 2018, the

246 corresponding week-1 climatology is based on the ensemble mean of the hindcast ensemble  
247 initialized on 23 July for each year from 1998 to 2017. The climatology is computed for each lead  
248 week separately, yielding a lead-time dependent climatology. Anomalies for the predictions are  
249 then computed by subtracting the model climatology from each ensemble member. For the earlier  
250 case studies, the climatology is computed over a 19-year hindcast period excluding the year of the  
251 case study to simulate an operational prediction setting. Anomalies for reanalysis are computed  
252 in a consistent way, by subtracting the daily mean climatology computed from reanalysis data for  
253 the same years that are used for computing the hindcast climatology for each case study. The use  
254 of anomalies for the model and reanalysis with respect to their respective climatologies provides a  
255 simple bias correction.

256 The temperature predictions are verified against the 2m temperatures from ERA5 reanalysis  
257 (Hersbach et al. 2020), as temperatures are well represented in reanalysis. Precipitation can  
258 show greater biases in reanalysis (Alexander et al. 2020), hence precipitation is verified against  
259 observational datasets from the Australian Water Availability Project (AWAP) 5 km daily gridded  
260 rainfall analysis (Jones et al. 2009) and the CPC Global Unified Gauge-Based Analysis of Daily  
261 Precipitation (Chen et al. 2008).

262 The temperature extremes case studies compare the probability density functions (PDFs) of the  
263 ensemble members for different lead weeks. Tercile limits (below-normal, normal, and above-  
264 normal, as well as the 10th and the 90th percentiles) are computed with respect to the lead  
265 time-dependent model climatology, based on 11 hindcast members. For the rainfall extremes,  
266 forecast performance is assessed by measuring the forecast system's association and discrimina-  
267 tion attributes, using the Spearman correlation coefficient (Wilks 2019) and the area under the  
268 Relative Operating Characteristic (ROC, Wilks 2019) curve for the above-normal category, re-  
269 spectively. The Spearman correlation is a non-parametric measure of how in-phase the forecasts

270 and observations are (correlation values of 1 indicate perfect association), and the ROC area  
271 for the above-normal category measures how well the forecast system discriminates between the  
272 above-normal and the other tercile-based categories, with values at 50% indicating a discrimination  
273 as good as that of climatology-based forecasts, and values above (below) 50% indicating better  
274 (worse) discrimination than climatology-based forecasts. The precipitation forecasts are calibrated  
275 according to a pattern-based Model Output Statistics approach using canonical correlation analysis  
276 (CCA; Tippett et al. (2008)), implemented via PyCPT, a set of Python libraries interfacing the  
277 Climate Predictability Tool (Muñoz 2020; Muñoz and Coauthors 2019; Mason et al. 2021), using  
278 IRI's "NextGen" forecast approach (Muñoz and Coauthors 2019; WMO 2020). To obtain a robust  
279 sample size, these metrics were computed using all 8 initializations (20 years per initialization)  
280 available for the months and target dates listed in Table 1, conducted independently for each rainfall  
281 extreme case study. For example, for the Guatemala case study (see next section), eight 20-year-long  
282 hindcasts were used, corresponding to all initializations available for June 1998-2017, providing a  
283 total of 160 hindcast weeks to compare against the corresponding 160 weeks of observed rainfall.

284 For additional details see Materia et al. (2020a).

285 For evaluating the model performance for the cyclones, their observed tracks are compared against  
286 the probability of cyclone occurrence given by the probability of a cyclone passing within 300 km  
287 of each grid point using the ECMWF tracker (Vitart et al. 1997) from the 51-member ensemble of  
288 the prediction system. The observed tropical cyclones data are obtained from the International Best  
289 Track Archive for Climate Stewardship (IBTrACS) (Knapp et al. 2010). The observed track for the  
290 medicane is obtained from the ECMWF operational analysis. The medicane is further evaluated  
291 using Convective Available Potential Energy (CAPE), an indicator of atmospheric instability, which  
292 is a necessary condition for the development of severe weather events. CAPE has been found to

293 be a prominent indicator and potential predictor for tropical cyclones (Huang and Liang 2010; Lee  
294 and Frisius 2018; Mylonas et al. 2018) but has not been prominently used for medicanes.

295 **3. Extreme event case studies**

296 This section presents specific case studies for the four types of extremes. The case studies  
297 were selected based on their extreme nature and societal impacts. While this selection should  
298 not be seen as a complete assessment of model performance or inter-comparison of predictability  
299 between event types or within the same event type, these case studies serve as a representative  
300 selection of extreme events and their predictability, which can translate into timescales of emergency  
301 preparedness (White et al. 2021). Table 1 provides an overview of the timing and location of each  
302 case study.

303 *a. Heatwaves*

304 We first examine the predictability of four extreme heatwaves in North America, Europe, and  
305 East Asia between 2013 and 2019 (Fig. 1). The first two heatwaves are part of the extreme Northern  
306 Hemisphere heatwave in summer 2018, when heatwaves simultaneously affected North America  
307 and Eurasia. We focus on the week of July 23-29, 2018, when temperatures over California reached  
308 51°C in Death Valley. California monthly mean temperatures for July surpassed the previous record  
309 set in 1931 (NOAA 2018) as heatwaves also occurred earlier that month. Similarly in Europe,  
310 the seasonal mean was strongly affected as the heat arrived in two waves, one from mid-May to  
311 mid-June and the second from mid-July to the beginning of August.

312 The model successfully predicts the concurrent 2018 heatwaves for the target period 3 weeks  
313 ahead in terms of the spatial structure of the anomalies for both considered regions, although  
314 with reduced amplitudes, meaning that most ensemble members remain well below the observed

315 anomalies (Fig. 1a-d). For Europe, at lead times of 2 weeks, 49 out of 50 ensemble members  
316 exceed the upper third of the climatological distribution (Fig. 2b). The forecast probability for the  
317 upper tercile is still 86% at lead times of 3 weeks and reduces to 60% for lead week 4, but with  
318 a long tail of the distribution towards extreme heat. For California, the model also predicts the  
319 extreme heat with some confidence out to 4 weeks (Fig. 2a). The 2-week lead forecast yields the  
320 most confident prediction, with 29% of ensemble members predicting temperatures above the 90th  
321 percentile, and 78% predicting above normal temperatures. Interestingly, although the 3-week  
322 lead forecast distribution is still shifted towards above normal temperatures, it is arguably the  
323 weakest prediction, with only 12% of members predicting temperatures above the 90th percentile,  
324 as compared to 24% for week 4.

325 Generally, California / western U.S. heat waves tend to be associated with high pressure over the  
326 Great Plains, low pressure off the California coast, and warm moist air transport from the south.  
327 There has been an increasing trend in this type of humid heatwave in recent years due to warming  
328 ocean temperatures (Gershunov and Guirguis 2015). When present, this ocean-atmosphere pattern  
329 can lead to higher predictability of heat waves, although forecast accuracy over the western U.S. and  
330 California is on average lower relative to other U.S. regions (Gershunov and Guirguis 2012; Ford  
331 et al. 2018; Kornhuber et al. 2019). However, July 2018 was atypical in that it was characterized  
332 by a wave-7 pattern (Kornhuber et al. 2019) associated with a strong and persistent region of high  
333 temperatures over much of the U.S. in the first half of July, and high pressure anomalies off the  
334 coast of and over the western U.S. in the last two weeks of July. Land - atmosphere and vegetation  
335 feedbacks are further suggested to have played a role in the 2018 heatwave, especially over central  
336 Europe (Liu et al. 2020; Sinclair et al. 2019; Albergel et al. 2019). Finally, the event was made  
337 more likely due to anthropogenic climate change (Yiou et al. 2019).

338 Less than a year after the devastating 2018 heatwave, another series of heatwaves affected the  
339 United States in 2019. In late May 2019 (we here consider the week of May 24 - 30), an early season  
340 heatwave affected the southeastern U.S., tied to a wavy jet stream pattern with anomalously high  
341 (low) pressure over the southeastern (southwestern) U.S. (Liberto 2019). The model captures the  
342 temperature anomalies at 3-week lead time, but it notably underestimates the extreme temperature  
343 anomalies (Fig. 1e,f), which is also found in the NCEP CFSv2 model (Luo and Zhang 2012). This  
344 underestimation is evident in the ensemble spread (Fig. 2c).

345 A further devastating heatwave was observed in East Asia in August 2013. The heatwave persisted  
346 for over two weeks from late July to mid-August, resulting in severe socio-economic losses in the  
347 region (Duan et al. 2013; Sun et al. 2014; Li et al. 2019). South Korea experienced the hottest  
348 summer nights and the second hottest summer days since 1954 (Min et al. 2014). In western Japan,  
349 daily maximum temperature records were broken or tied at 143 weather stations (JMA 2013), many  
350 of which were broken again during the 2018 heatwave. The extreme persistence and severity of the  
351 event resulted from the combination of a westward extension of the North Pacific subtropical high  
352 (Jing-Bei 2014; Li et al. 2015) and a zonal wave train (Yeo et al. 2019) resembling the circumglobal  
353 teleconnection (Ding and Wang 2005).

354 For the considered target week of 5-11 August 2013, a warm anomaly of over 4°C was observed  
355 in the large metropolitan areas of eastern China, while the heatwave extended to the Korean  
356 peninsula and Japan (Fig. 1g). The temperature anomaly was larger in the urban areas than in  
357 rural areas (Wang et al. 2017), possibly due to the urban heat island effect. The temperature  
358 distribution is well captured by the model over land at a 3-week lead time, though the magnitude  
359 is slightly underestimated, while the warm anomaly over the eastern China Sea is not reproduced  
360 (Fig. 1h). When initialized four weeks before the target period on July 15, more than a third  
361 of the ensemble members point to below normal temperatures, although twenty percent already

362 predict temperatures above the 90th percentile (Fig. 2d). However, starting at the 3-week lead  
363 time, essentially all ensemble members predict above normal temperatures, and only one ensemble  
364 member at 2-week lead time predicts temperatures below the 90th percentile. More importantly, the  
365 ensemble-mean of these initializations quantitatively well captures the observations (i.e., individual  
366 ensemble members are well centered about the observed value). This result indicates that the 2013  
367 East Asia heatwave is quantitatively well predicted by the model at a maximum lead time of three  
368 weeks.

369 *b. Cold spells*

370 Several examples of extreme cold spells in Europe are studied in this section. We start with a  
371 cold spell in eastern and southeastern Europe in late winter and early spring of 2003 (Levinson  
372 and Waple 2004) that preceded a record-breaking summer heatwave. The month of February was  
373 the coldest on record in Albania and Macedonia, and temperatures in southeastern Europe were  
374 between -2°C and -5°C below normal for much of February and early March (Dittmann et al.  
375 2004). The target week of April 3-9 (Fig. 3a) marked the end of this cold period, but was cold  
376 enough that the month of April registered record minimum temperatures in the Baltic region, the  
377 Danube watershed, and part of Italy and the Balkans (Dittmann et al. 2004). The extreme cold  
378 was associated with atmospheric blocking over the UK leading to southward advection of cold  
379 air masses from the Arctic, reaching southeastern Europe on April 7. The temperature contrasts  
380 between the frigid air mass and the southern Adriatic Sea caused strong convective precipitation,  
381 with heavy snowfall along the coasts of western Greece, Albania and southern Italy.

382 The model predicts the cold anomaly in central Europe (Fig. 3b), though with a southeastward  
383 shift and smaller anomalies than observed. The ensemble starts encompassing the observed  
384 anomaly at the 3-week lead time (March 19 initialization, Fig. 4a), indicating a 51% probability of

385 temperatures in the lower tercile for the target week, and a 29% chance of temperatures below the  
386 tenth percentile. At the 2-week lead time, the confidence about the occurrence of cold weather is  
387 clearly increased, with 72% of the ensemble members indicating temperatures below normal, and  
388 53% below the 10-percentile threshold.

389 Another cold spell preceding a hot summer occurred in late February / early March 2018 in  
390 central and western Europe after an otherwise mild winter. The cold wave was likely linked to a  
391 major SSW event in mid-February 2018, which enhanced the probability of the negative NAO and  
392 Greenland blocking during the peak of the cold event (Kautz et al. 2020). The SSW itself was  
393 anticipated 10 days ahead (Karpechko et al. 2018) – a typical predictability timescale for SSWs  
394 (Domeisen et al. 2020a). Knight et al. (2021) identified the extreme MJO event of January 2018  
395 as an important driver of this SSW.

396 The blocking associated with this cold spell shows predictability in the ECMWF system (Ferranti  
397 et al. 2019). The forecast initialized on February 12, 2018, the day of the SSW event (a lead time of  
398 around 3 weeks), captures the cold anomaly over central Europe and part of the British Isles, but the  
399 anomaly is significantly underestimated (Fig. 3c,d). Already at 4 weeks lead time (initialization on  
400 February 5) the most likely category is the below normal tercile (with 54% of ensemble members)  
401 for temperature over western Europe (Fig. 4b). Further analysis using North Atlantic weather  
402 regimes suggests that the sequence of weather regimes before and during the cold spell (positive  
403 NAO, blocking, followed by negative NAO, as documented in Kautz et al. (2020)) were correctly  
404 anticipated by the model from the February 12 start date (not shown).

405 Another cold spell linked to atmospheric blocking occurred in winter 2016/2017 (Fig. 3e). The  
406 block over Europe brought warm air to Scandinavia and Arctic air to eastern–central Europe in  
407 the second week of January (Magnusson 2017). A cut-off low developed, causing exceptionally  
408 low temperatures in the Balkan Peninsula as well as snowfall in Greece and southern Italy with

409 significant socioeconomic impacts due to the long duration of the event (Anagnostopoulou et al.  
410 2017). The following week (16-22 January 2017), central Europe was affected by further cold air  
411 advection due to a tripole in surface pressure, with high pressure from the UK towards the Black  
412 Sea, and low pressure in the western Mediterranean and to the north of Scandinavia. This tripole  
413 was consistent with quiescent, cold and dry conditions over central Europe in the region of the  
414 anticyclone (Fig. 3e).

415 The forecast issued on January 2 (3-week lead time) already indicates an enhanced probability of  
416 below normal temperatures (Fig. 3f). Four weeks before the event, the probability for temperatures  
417 in the lower tercile already reaches 45% and increases to 63% (89%) at 3 (2) weeks before the  
418 event (Fig. 4c). The ensemble clearly narrows towards the observed anomaly at shorter lead times.

419 The probability of temperature anomalies below the 10th percentile increases closer to the event,  
420 from 18% (4 weeks before), to 29% (3 weeks before), and finally to 64% 2 weeks before the event.

421 The cold spell produced a peak in electricity demand, particularly in France, where most of the  
422 heating is powered by electricity. The concomitant low wind speeds led to a lower than normal  
423 wind power generation, and several nuclear power plants in France were under maintenance (RTE  
424 2017). This combination caused a high-risk situation for France's energy system that could have  
425 been better managed given the forecasts, for example through a postponement of the planned  
426 maintenance operations in the nuclear power plants.

427 Another extreme cold spell occurred in late 2010. From late November to early December 2010,  
428 Germany and France recorded the coldest December in 40 years, while in the United Kingdom  
429 this was the coldest December in 100 years (Fig. 3g). December 2010 was characterized by an  
430 unusually strong negative NAO (Maidens et al. 2013) with strong cold air advection from northern  
431 Europe and Siberia (Prior and Kendon 2011). The cold anomaly over land was accompanied by  
432 a marine cold air outbreak (MCAO, according to the MCAO index used in Afargan-Gerstman

433 et al. (2020)) in the Norwegian and the Barents Seas. MCAOs can have devastating impacts on  
434 marine infrastructure and offshore activities, for example by creating favorable conditions for the  
435 formation of polar lows (Rasmussen 1983; Kolstad et al. 2009; Noer et al. 2011; Landgren et al.  
436 2019). Indeed, a polar low was detected in satellite imagery in the Norwegian Sea off the coast  
437 of Norway on the 25th of November 2010, two days before our selected target date, based on the  
438 STARS database of polar lows (<http://polarlow.met.no/>), but no records regarding damages  
439 from this polar low have been found. Although the occurrence of cold air outbreaks in the North  
440 Atlantic and over northern Europe is often associated with stratospheric weak polar vortex events  
441 (e.g., Kolstad et al. 2010; Afargan-Gerstman et al. 2020), this event is unlikely to have been driven  
442 by the stratosphere, possibly reducing its predictability.

443 Cold anomalies had been predicted for northern Europe 3 weeks earlier by the hindcast initialized  
444 on November 11, however the prediction clearly underestimates the magnitude of the observed event  
445 (Fig. 3g,h). Hindcasts for lead times beyond 3 weeks (initialization on Nov 4) already provide  
446 an indication of the cold anomaly, with probabilities around 20% for temperatures below the  
447 10th percentile. Hindcasts initialized at lead times of 2 and 3 weeks capture the below normal  
448 temperatures with a probability of above 90% and 50%, respectively (Fig. 4d). Hence, although  
449 the probability of a cold extreme is significantly increased already 3 weeks before the event, the  
450 magnitude of the extreme event is only captured at 2-weeks lead time.

451 *c. Precipitation events*

452 In this section we focus on four events with anomalous precipitation in Central and South  
453 America, Europe, and Australia. The first considered event is analyzed in the context of a volcanic  
454 eruption, as an example of using subseasonal forecasts for compound events, where the possibility  
455 of heavy rainfall was of concern. Guatemala's Volcán de Fuego, a stratovolcano, erupted on June

456 3rd 2018, killing at least 113 people, while more than 300 remained unaccounted for (Program  
457 2018). Ash plumes and pyroclastic flow material affected communities up to 25 km away from  
458 the volcano. The pyroclastic flows produced lahars (i.e., mudflow or debris flow) intermittently  
459 for several weeks, leading to evacuations of the nearby communities and displacing thousands of  
460 Guatemalans, destroying infrastructure and damaging crops. Overall, the eruption impacted 1.2  
461 million Guatemalans, and cost more than U.S.D\$219 millions (CEPAL 2018; CONRED 2018;  
462 WorldBank 2018).

463 The impacts could have been worse if precipitation, which typically peaks in the region in June,  
464 had been higher. Intense or persistent rainfall events (a) tend to make lahar viscosity thinner, which  
465 sustains the flow of pyroclastic debris for a longer duration, potentially causing more damage; (b)  
466 can remobilize unconsolidated pyroclastic deposits, causing post-eruption lahars; (c) can displace  
467 hanging slabs of solidified mud, debris and boulders down steep slopes, with the potential to destroy  
468 infrastructure and kill people; and (d) tend to interfere with evacuation, search and rescue, cleaning,  
469 and rebuilding operations. Due to the activities deployed at the time in Guatemala by the Columbia  
470 University World Project “Adapting Agriculture to Climate Today, for Tomorrow” (IRI 2018),  
471 the International Research Institute for Climate and Society and INSIVUMEH – the Guatemalan  
472 national meteorological agency – started working together immediately after the eruption to provide  
473 calibrated subseasonal rainfall forecasts from the prediction system to the National Government  
474 and a wide variety of local institutions.

475 Calibrated rainfall NextGen forecasts (Muñoz and Coauthors 2019) initialized on June 4 in-  
476 dicated low chances of exceeding the weekly median for the following four weeks for most of  
477 Guatemala ( compare to Fig. 5a,b; Fig. 6a,b), and further analysis for the location of interest helped  
478 INSIVUMEH advise government institutions on evacuation, search and rescue, and cleaning and  
479 rebuilding operations. Subsequent weekly forecast updates confirmed the original expected out-

480 comes. These results build evidence on the advantages of using real-time subseasonal rainfall  
481 forecasts to help decision makers during and after volcanic eruptions, and potentially other seismo-  
482 logic and compound environmental events. Using a combination of forecasts at multiple timescales  
483 is suggested to be an optimal practice in these cases, consistent with the “Ready-Set-Go” approach  
484 (Goddard et al. 2014).

485 Another event of interest occurred in January 2016, when a series of heavy precipitation events  
486 affected Northwestern South America, leading to widespread flooding in coastal northern Ecuador,  
487 especially in the Province of Esmeraldas. The flood displaced 120 families, left one casualty, and  
488 was the largest such event in 20 years (Davies 2016). The flooding was associated with an early  
489 onset of the heavy rainfalls and severe mesoscale convective systems (MCSs) that would normally  
490 not be expected until annual precipitation peaks in April / May (Mohr and Zipser 1996; Bendix  
491 et al. 2009). On January 25, convective storms developed into a MCS with an extent of around  
492 250 km over the western Andes foothills of the Esmeraldas river basin, a region of abundant low-  
493 level moisture bounded by the Andes. This heavy precipitation event was favored by interactions  
494 between the very strong El Niño event and an unusually persistent MJO in phases 2 and 3 (Pineda  
495 et al. 2021).

496 Weekly ensemble-mean rainfall anomaly hindcasts represent the spatial pattern of the anomalous  
497 precipitation extreme over the catchment over all lead times (Fig. 5c,d), with the best event  
498 identification for week 3 initialized on 28th Dec 2015 (i.e., the week 3 anomaly was closer to  
499 the observations as compared to week 2 (not shown)). For the Esmeraldas river basin the ROC  
500 scores for week 3 range from 0.5 to 0.6 (Fig. 6c), indicating low to modest discrimination of the  
501 above-normal rainfall on January 25th. The Spearman-rank correlations range from -0.25 to 0.25  
502 (Fig. 6d); thus, based on the hindcast, the model performance is limited for the region where the  
503 extreme rainfall occurred at a lead time of 3 weeks. However, the positive precipitation anomaly

504 of more than one standard deviation averaged over the grid points closest to the catchment was  
505 captured for all lead times of 1-3 weeks (Pineda et al. 2021). Therefore, the use of the S2S  
506 rainfall forecast could have provided decision-makers with useful information about the onset of  
507 this extreme precipitation event. A timely uptake of the available forecasts 2-3 weeks in advance  
508 by the National Met-Hydro Service could have allowed for an early warning for this catastrophic  
509 flood event.

510 Another heavy precipitation event affected northwestern Italy (Piedmont and Liguria) in the  
511 period from 21 - 25 November 2016. Over these 5 days, more than 50% of annual precipitation  
512 was recorded in several areas, with peaks above 600 mm (ARPA Liguria 2017; ARPA Piemonte  
513 2017). Severe damage was caused by river floods with flow-rate return times up to 200 years,  
514 and widespread occurrence of shallow landslides (Cremonini and Tiranti 2018). This episode  
515 developed in the middle of a persistent drought affecting most of central and western Europe in  
516 2016/2017 (García-Herrera et al. 2019). The precipitation anomaly is underestimated by the model  
517 and exhibits a misplaced maximum for the forecast initialized on 7 November 2016 for week 3  
518 (lead times 15–21 days, Fig. 5e,f). However, the positive anomaly over northwestern Italy is  
519 reproduced more than 2 weeks in advance. Positive anomalies were also correctly located in the  
520 Western Mediterranean region. These anomalies are significantly different at the 10% level from  
521 the ensemble climatology according to a Wilcoxon–Mann–Whitney test (not shown).

522 The large-scale mid-tropospheric configuration leading to this precipitation event was charac-  
523 terized by a persistent low pressure anomaly over the Iberian Peninsula, surrounded by areas of  
524 high pressure extending from the North Atlantic to Eastern Europe (ARPA Piemonte 2017). This  
525 dipole in pressure anomalies favors meridional moist advection across the complex orography  
526 downstream, leading to heavy precipitation in the Mediterranean in this season (e.g., Buzzi et al.  
527 2014; Khodayar et al. 2018). The anomalous persistence of the large-scale pattern likely favored

528 the predictability of the event (Vitart et al. 2019). Although the verification scores of the week-3  
529 forecasts for this area (Fig. 6e,f) indicate, on average, a relatively low predictive performance,  
530 the sufficiently correct representation of the atmospheric dipole in the extended range may have  
531 enhanced the predictability of precipitation for this event. Similarities are found with the historical  
532 Piedmont 1994 flood (Davolio et al. 2020), when heavy precipitation was triggered by a similar  
533 but less persistent large-scale pattern.

534 The last precipitation extreme considered here investigates extreme rainfall, strong winds and  
535 below normal daytime temperatures over tropical northeastern Australia in early February 2019.  
536 The event caused wide-spread infrastructure damage, coastal inundation to homes, and destroyed  
537 over 500,000 livestock, predominantly beef cattle (losses were in the dark green areas in Fig. 5g).  
538 The total economic loss was estimated at \$5.68 billion AUD (Deloitte 2019). The extreme  
539 rainfall was associated with a quasi-stationary monsoon depression that lasted around 10 days,  
540 with weekly rainfall totals above 1000 mm in some locations, maximum temperatures of 8-12°C  
541 below average, and sustained winds between 30 to 40 km/h (Bureau of Meteorology 2019). The  
542 event was associated with an active MJO that stalled over the western Pacific (Cowan et al. 2019).  
543 Even though most of the predictability in extreme austral summer precipitation for northeastern  
544 Australia comes from equatorial Pacific SSTs (King et al. 2014), ENSO conditions were neutral and  
545 likely did not contribute to this event. Consistent with the neutral ENSO conditions, the Australian  
546 Bureau of Meteorology issued a monthly rainfall outlook for February with little indication of the  
547 impending event. Only in the week prior to the event, the Bureau's dynamical prediction system,  
548 the Australian Community Climate Earth-System Simulator-Seasonal version 1 (ACCESS-S1),  
549 predicted a more than doubled likelihood of extreme rainfall (Cowan et al. 2019).

550 The operational real-time forecasts initialized on 17 January 2019 (i.e., a week 3 forecast) confirm  
551 the above analysis (Fig. 5h). The region with the highest observed rainfall accumulations (blue

552 box in Fig. 5g) has a ROC score between 0.4 and 0.6, indicating low model performance (Fig. 6g).  
553 Likewise, wide-spread Spearman-rank correlations of between 0 and 0.25 (Fig. 6h) provide further  
554 evidence that the week 3 forecast does not predict the extreme rainfall week. This confirms separate  
555 results from eleven S2S models that suggest the rainfall event's very extreme nature could not be  
556 predicted with certainty more than a week ahead (not shown).

557 *d. Cyclones*

558 We here analyze the subseasonal predictability of four cyclones (three tropical cyclones and one  
559 medicane). While all selected tropical cyclones occurred in different regions, all were associated  
560 with an active MJO, as discussed below.

561 As a first case we investigate tropical cyclone (TC) Claudia (Fig. 7a) in the western part of the  
562 Australian basin classified as a severe TC in the Australian scale. TCs in the western part of the  
563 Australian basin represent an important challenge to the oil industry since the majority of Australian  
564 oil rigs are located in this region. Therefore, the predictability of tropical cyclones a few weeks in  
565 advance in western Australia has important economic value, as well as societal impact in the case  
566 of landfall. Climatologically, 5.2 cyclones occur in that sub-basin per season, with 2.6 reaching  
567 severe TC intensity and 1.2 making landfall in Australia (Chand et al. 2019). The Australian  
568 TC season typically lasts from November to April, with a peak in January to March. Claudia's  
569 characteristics (e.g., lifetime, latitude of genesis, maximum intensity and dissipation) were very  
570 typical of western Australia TCs (Chand et al. 2019). Claudia developed over Indonesia's Maluku  
571 Island on 4 January 2020 and moved south-westward along the northwestern coast of Australia for  
572 about 2 weeks (including a period as a tropical depression) (Fig. 7a,b). It reached a peak intensity  
573 of 968 hPa (140 km/h) on January 13.

574 The prediction system initialized on 30 December 2019 predicted probabilities of up to 40% for  
575 a TC north-west of Australia for lead times of 15-21 days (week 3) (Fig. 7b) – significantly higher  
576 than the climatological probability (about 5%) for this season. Although the observed TC track  
577 is located slightly north of the area of maximum probability, this result suggests that the forecast  
578 could have provided a useful early warning for this TC. While other models from the S2S database  
579 also predicted an increased risk of TC activity in this region, the multi-model ensemble probability  
580 of TC strike was only around 10-20%. Claudia coincided with an exceptionally intense MJO (3  
581 standard deviations above climatology of the RMM index (Wheeler and Hendon 2004)) over the  
582 Maritime Continent and warm SST anomalies over the eastern Indian Ocean. This combination is  
583 likely to have contributed to make this intense and long-lasting tropical cyclone more predictable  
584 than usual.

585 Another recent example of a well-predicted system is cyclone Belna (Fig. 7c) just a few months  
586 earlier. Belna formed to the north of the Mozambique channel and eventually moved southward.  
587 Cyclones occur in the channel on average twice per year (Kolstad 2021). Over recent years, multiple  
588 tropical cyclones made landfall in that region (Idai and Kenneth in 2018/19 and Chalane, Eloise,  
589 Guambe and Iman in 2020/21), leading to devastating floods in Mozambique and neighboring  
590 countries (Emerton et al. 2020).

591 For cyclone Belna (Fig. 7c), the model prediction initialized on 18 November predicts a prob-  
592 ability of cyclone occurrence of up to 30% in the Mozambique Channel at the remarkable lead  
593 time of four weeks (Fig. 7d). On 5 December, 17 days after forecast initialization, the system  
594 was upgraded to a tropical storm and named. On 7 December it attained hurricane intensity, and  
595 a day later it passed near the Mayotte Islands in the northernmost part of the Channel. It made  
596 landfall in Madagascar on 9 December, to the east of the predicted path (Fig. 7d), and it dissipated  
597 over land two days later. A reason for the successful long-range prediction of Belna is likely the

598 strong MJO envelope within which Belna formed (letter B in Fig. 8c), although the MJO was not  
599 successfully predicted thereafter. The model forecast (Fig. 8d) indicates enhanced convection in  
600 that area, particularly in early December when Belna developed. The very intense TC Ambali  
601 (marked "A" in Fig. 8c) also formed near the MJO envelope just to the east of Belna.

602 Another TC associated with an intense MJO event occurred during a period of unusually high TC  
603 activity in the West Pacific. In early June 2015, an MJO convective envelope developed over the  
604 Indian Ocean, intensified and propagated eastward reaching an amplitude of 2.58 in the Realtime  
605 OLR MJO Index (ROMI) (Kiladis et al. 2014). Only two other MJO events during June and July  
606 in the period 1979-2018 reached this amplitude. This MJO event provided favorable conditions  
607 for TC formation leading to the genesis of typhoons Linfa, Chan-hom (Fig. 7e), and Nangka over  
608 the Western North Pacific, exemplified by the observed OLR anomalies and MJO-filtered OLR  
609 anomalies (Fig. 8a). Typhoons Linfa, Chan-hom, and Nangka (denoted by letters C, L, and N)  
610 in late June and early July formed soon after the passage of the MJO envelope. All three storms  
611 would go on to make landfall; Chan-hom was responsible for the second highest damages (1.5  
612 billion U.S.D) in the West Pacific that season (Camargo 2016). Additional TCs in both the Indian  
613 Ocean and West Pacific were associated with this MJO event (Fig. 8a).

614 The ensemble forecast initialized on June 15, 2015 (0000Z, Fig. 7f) indicates the increased  
615 probability of a TC during week 4 of the forecast (valid July 7-13) in this area. The tracks of  
616 typhoons Linfa, Chan-hom, and Nangka (from west to east) overlap this area of enhanced TC  
617 formation probability. The forecast also captures the eastward propagation of the MJO envelope  
618 (Fig. 8b), although the MJO amplitude is weaker than observed.

619 As a last case we investigate a medicane, specifically the *Mediterranean Cyclone 2018 - M02*  
620 Zorbas (Fig. 7g). The medicane developed on September 27, 2018 in the eastern Mediterranean  
621 Sea between Sicily and Southern Greece and gradually intensified, developing characteristics of a

622 tropical cyclone. As for many medicanes, its origin was related to a potential vorticity streamer  
623 (Miglietta et al. 2017). On September 29, the storm made landfall at peak intensity in Kalamata,  
624 Peloponnese, Greece, with a pressure of 989 hPa and sustained winds of 120 km/h (approx. 33  
625  $\text{m s}^{-1}$ ). The event was associated with a Dvorak number of T4.0 (Service 2019; ECMWF 2019),  
626 corresponding to a marginal category 1 hurricane.

627 The initialization on September 13, 2018 predicts a region of formation shifted to the west  
628 compared to the actual area of event formation (Gulf of Sirte, Libya) (Fig. 7h). While the low  
629 probability of formation is an indication of the difficulty of predicting such a rare event, the  
630 climatological probability of cyclone formation in the model in this region is less than 1%, hence  
631 the displayed chance of a cyclone in this region is clearly above the expected probability. In  
632 addition, the prediction shows low probability for the event to follow the observed path (black  
633 line) towards Greece. One of the reasons for the limited predictability of the event was likely the  
634 uncertainty in the initial conditions near an upper-level jet streak over the Gulf of Saint Lawrence  
635 (Portmann et al. 2019).

636 However, predictability may potentially be improved using CAPE (see section 2). For an  
637 initialization of the model as early as August 30, 2018 and a validation on September 26, 2018,  
638 very high values of CAPE are found in the formation region of medicane Zorbas (Fig. 8). Hence,  
639 CAPE provides evidence of a medicane 3-4 weeks prior to its formation. Further analysis is needed  
640 to assess the full predictability capabilities of CAPE for medicanes.

#### 641 **4. General Discussion and Outlook**

642 We have here demonstrated subseasonal predictability for selected case studies of some of the  
643 most prominent and impactful extreme events globally, namely heatwaves, cold spells, precipitation  
644 events, and cyclones. Heatwaves tend to be the most predictable among the extreme events

645 considered. The prediction system can often anticipate the anomalous temperature 3-4 weeks in  
646 advance, though often with a reduced amplitude. Cold spells also often show an indication of  
647 predictability, generally at lead times of 2-3 weeks. Precipitation events tend to be less predictable,  
648 but if the large-scale circulation associated with a large-scale driver (e.g., an active MJO) is  
649 successfully captured, predictability of 2-3 weeks can be obtained. For tropical cyclones, their  
650 formation region and tracks can often be anticipated 3 weeks in advance provided a successful  
651 prediction of strong MJO events. Furthermore, CAPE shows promise for indicating tracks and  
652 formation regions for extratropical cyclones. Note that these conclusions are based on the here  
653 documented case studies, and although the predictability and conclusions obtained here agree with  
654 other published results, it is likely that individual events may be much more or less predictable  
655 depending on the region, type, and amplitude of the event. Therefore, in addition to differences in  
656 predictability between different types of extremes there are important differences in predictability  
657 within the same event type. In the here demonstrated case studies, these inter-event differences hint  
658 at different processes and precursors responsible for forcing, modulating, or amplifying certain  
659 extreme events of the same type, including remote drivers such as the MJO.

660 We would like to emphasize that the case studies presented here do not represent a comprehensive  
661 evaluation, hence the predictability shown for these events may differ from a systematic evaluation  
662 across a larger number of events. Hence, while this study only investigates a limited number of  
663 extreme events as case studies, systematic studies of inter-event differences in predictability will  
664 be required to better understand the role of the identified drivers. In particular, extreme events with  
665 a common remote driver could be cross-compared in order to more clearly evaluate the driver's  
666 role (or, in fact, its absence). These studies should also include an investigation of false alarms,  
667 that is, extreme events triggered by remote drivers and predicted in the model that do not verify in  
668 observations.

669 An improved process understanding of the drivers of extremes and their representation in predic-  
670 tion systems as well as the development of post-processing techniques will continue to significantly  
671 benefit the subseasonal prediction of extreme events. On the other hand, even with significant model  
672 improvements, many extremes will retain an inherent unpredictability related to the chaotic na-  
673 ture of the climate system. Still, understanding why and when certain extreme events are more  
674 predictable than others will help to identify and use windows of opportunity, that is, atmospheric  
675 states with enhanced predictability. Event-based and region-specific knowledge of the level of  
676 predictability of the relevant processes and the related extreme events will significantly benefit  
677 stakeholders and users of extreme weather data.

678 While this study has focused on a single prediction system from the ECMWF, an increasing  
679 number of multi-model studies for the prediction of specific extremes are currently becoming  
680 available (e.g. Li et al. 2021; Materia et al. 2020b; Domeisen et al. 2020b), highlighting inter-model  
681 differences rather than inter-event differences, which were the focus of this study. Furthermore,  
682 bias correction and calibration methodologies that refine the forecast's statistical properties based  
683 on a reference period will further enhance these forecasts. In this study we used anomalies in order  
684 to correct the systematic bias and model drift, keeping in mind that this might affect the chance of  
685 the model to predict, for example, hot versus cold spells, especially for longer lead times. However,  
686 region- and process-specific biases and drifts are likely still present in our analysis. In addition,  
687 standard bias-correction applied here is "unfair" (Risbey et al. 2021), since it uses observed data  
688 that would not be available to a real-time forecast: in fact, in several cases the observations used  
689 for the climatology occur after the forecast starts, and the hindcast therefore contains artificial skill.  
690 This can be misleading for users who must take decisions using real forecasts, which are likely to  
691 exhibit lower forecast skill than what is commonly shown in research studies.

692 In addition, a wider range of model evaluation and bias correction techniques are available,  
693 with the most relevant choices depending on the variable and on the desired characteristics for the  
694 output (see Torralba et al. (2017) and Manzanas et al. (2019) for a comparison of methodologies  
695 for seasonal predictions and Wernli et al. (2008); Dorninger et al. (2018) for forecast evaluation  
696 techniques on deterministic timescales). Although some standard methods and tools are starting to  
697 be used more widely (Muñoz 2020; Muñoz and Coauthors 2019), implementation at subseasonal  
698 timescales is non-trivial and requires a robust climatological reference to be successful (Manrique-  
699 Suñén et al. 2020). One of the challenges is the limited amount of model data available for the  
700 reference period (short hindcast periods and few ensemble members). Examples of implementation  
701 of bias-correction methodologies for subseasonal predictions can be found in Monhart et al. (2018)  
702 and Manrique-Suñén et al. (2020). These statistical adjustments are of particular importance in  
703 sectoral applications (Materia et al. 2020a; DeMott et al. 2021; DiSera et al. 2020), when S2S  
704 predictions are used as input in impact models to calculate sector-relevant indicators or derived  
705 variables (e.g., energy production or agricultural yield (White et al. 2021)). As S2S predictions  
706 increasingly make their way into risk-based decision-making contexts, a continued development  
707 and assessment of subseasonal models, calibration techniques, and combination with other tools  
708 will significantly benefit these applications (Goddard et al. 2014; White et al. 2021).

709 Lastly, it remains difficult to quantify the economic value of S2S forecasts. In fact, even for  
710 very skillful forecasts, there can be significant economic losses that depend on factors beyond the  
711 forecasts themselves, involving the emergency response and preparedness of the affected region.  
712 However, it is clear that skillful forecasts on sub-seasonal to seasonal timescales can indeed add  
713 economic value, as has been shown for both temperature and cyclone predictions (Dorrington et al.  
714 2020; Emanuel et al. 2012).

715 In summary, this work is meant to showcase the importance of subseasonal forecasts in the  
716 development and improvement of a large variety of climate services. Therefore, it is difficult  
717 to homogenize across event type, forecast quality metrics, and prediction format (deterministic  
718 versus probabilistic). By their own nature, distinct events in different locations of the world require  
719 different verification tools, and time aggregations must be meaningful to users. This study goes  
720 towards this direction by starting to address the recommendations for advancing the S2S forecast  
721 verification practices recently highlighted by Coelho et al. (2019): Appropriate verification methods  
722 to deal with extreme events, novel verification measures specifically adapted for S2S forecasts, and  
723 enlargement of the sample size to address sampling uncertainties. All of these techniques are  
724 meant to build knowledge about the strengths and weaknesses of forecasts, and eventually increase  
725 confidence in S2S products among forecasters and users (Coelho et al. 2018).

726 As the performance of prediction models for extreme events at subseasonal lead times continues  
727 to increase with improvements in the understanding of extreme events and their representation  
728 in models, the here documented extreme events can be viewed as demonstrations and examples  
729 of this progress, which reaches far beyond these case studies, contributing to build or strengthen  
730 (depending on the case) a robust ecosystem of climate services (Goddard et al. 2020).

731 *Acknowledgments.* Support from the Swiss National Science Foundation through project  
732 PP00P2\_170523 to D.D., H.A.-G. and O.W. is gratefully acknowledged. In addition, support  
733 from the Swiss National Science Foundation through project PP00P2\_198896 to D.D. is gratefully  
734 acknowledged. H.A.-G. also acknowledges funding from the European Union’s Horizon 2020 re-  
735 search and innovation programme under the Marie Skłodowska-Curie grant agreement No 891514.  
736 Á.G.M., C.G.R. and D.P. were partially supported by the Columbia World Project “ACToday”,  
737 at Columbia University in the City of New York (<https://iri.columbia.edu/actoday/>);

738 Á.G.M. was also partially supported by the NOAA grant NA18OAR4310275. A.M.-S., L.L, L.P.,  
739 H.B., P.G., A.C.-P., D.B. and A.S. acknowledge funding from the European Union's Horizon 2020  
740 research and innovation programme under Grant 7767874 (S2S4E). SJC acknowledges support  
741 of NOAA S2S project NA16OAR4310079. TC is supported by the Northern Australian Climate  
742 Program (NACP). DT and HM are supported by the National Institute of Food and Agriculture  
743 Hatch project (Accession No. 1012578). S.-W.S. and H.K. are supported by the Basic Science  
744 Research Program through the National Research Foundation of Korea (2017R1E1A1A01074889).  
745 L.E.P acknowledges support of Corporación Ecuatoriana para el Desarrollo de la Investigación y la  
746 Academia (CEPRA grant). We acknowledge the use of the CSTools software package (Perez-Zanon  
747 et al. 2019) and R (R Core Team 2015) to produce figures 2 and 4.

748 *Data availability statement.* ERA5 reanalysis data was obtained from the Copernicus Cli-  
749 mate Change Service Climate Data Store (CDS), <https://cds.climate.copernicus.eu/cdsapp#!/home>.  
750 The ECMWF S2S model data was obtained through the MARS archive ([https://apps.  
751 ecmwf.int/datasets/data/s2s/](https://apps.ecmwf.int/datasets/data/s2s/)). CPC Global Unified Precipitation data were pro-  
752 vided by the NOAA/OAR/ESRL PSL, Boulder, Colorado, U.S.A, from their Web site at  
753 [https://www.psl.noaa.gov/thredds/catalog/Datasets/cpc\\_global\\_precip/catalog.html](https://www.psl.noaa.gov/thredds/catalog/Datasets/cpc_global_precip/catalog.html). Australian  
754 precipitation data from the Australian Water Availability Project (AWAP) is available on re-  
755 quest from the Bureau of Meteorology at [http://www.bom.gov.au/climate/austmaps/metadata-  
757 daily-rainfall.shtml](http://www.bom.gov.au/climate/austmaps/metadata-<br/>756 daily-rainfall.shtml). The satellite image for tropical cyclone Claudia was cap-  
758 tured by NOAA-20 satellite's IITS instrument [[https://www.nesdis.noaa.gov/content/tropical-  
759 cyclone-claudia-loses-strength-it-moves-away-australia](https://www.nesdis.noaa.gov/content/tropical-<br/>cyclone-claudia-loses-strength-it-moves-away-australia)]. The satellite image for cy-  
760 clone Belna was obtained from [https://en.wikipedia.org/wiki/Cyclone\\_Belna](https://en.wikipedia.org/wiki/Cyclone_Belna) [NASA:  
<https://worldview.earthdata.nasa.gov/>]. The satellite image for typhoon Chan-Hom was ob-

761 tained from [https://en.wikipedia.org/wiki/Typhoon\\_Chan-hom\\_%282015%29](https://en.wikipedia.org/wiki/Typhoon_Chan-hom_%282015%29) [SSEC/CIMSS,  
762 University of Wisconsin–Madison]. The satellite image for medicane Zorbas is  
763 a MODIS image captured by NASA’s Terra satellite (EOSDIS Worldview) from  
764 [https://commons.wikimedia.org/wiki/File:Zorbas\\_2018-09-29\\_0912Z.jpg](https://commons.wikimedia.org/wiki/File:Zorbas_2018-09-29_0912Z.jpg). The ECMWF CAPE  
765 data for studying medicane Zorbas were obtained from the IRI/LDEO Climate Data Library  
766 (<https://iri.columbia.edu/SOURCES/.ECMWF/.S2S>). Observed tropical cyclone data are  
767 obtained from the International Best Track Archive for Climate Stewardship (IBTrACS) (Knapp  
768 et al. 2010) at <https://climatedataguide.ucar.edu/climate-data/ibtracs-tropical-cyclone-best-track-data>.

## 770 References

771 Afargan-Gerstman, H., I. Polkova, L. Papritz, P. Ruggieri, M. P. King, P. J. Athanasiadis, J. Baehr,  
772 and D. I. Domeisen, 2020: Stratospheric influence on north atlantic marine cold air outbreaks  
773 following sudden stratospheric warming events. *Weather and Climate Dynamics*, **1 (2)**, 541–553.

774 Albergel, C., and Coauthors, 2019: Monitoring and Forecasting the Impact of the 2018 Summer  
775 Heatwave on Vegetation. *Remote Sensing*, **11 (5)**, 520.

776 Alexander, L. V., M. Bador, R. Roca, S. Contractor, M. G. Donat, and P. L. Nguyen, 2020:  
777 Intercomparison of annual precipitation indices and extremes over global land areas from in situ,  
778 space-based and reanalysis products. *Environmental Research Letters*, **15 (5)**.

779 Anagnostopoulou, C., K. Tolika, G. Lazoglou, and P. Maheras, 2017: The exceptionally cold  
780 January of 2017 over the Balkan Peninsula: A climatological and synoptic analysis. *Atmosphere*,  
781 **8 (12)**, doi:10.3390/atmos8120252, URL [www.mdpi.com/journal/atmosphere](http://www.mdpi.com/journal/atmosphere).

782 ARPA Liguria, 2017: Rapporto di evento meteoidrologico del 20-25/11/2016.  
783 Tech. rep. URL [http://www.arpal.liguria.it/contenuti\\_statici/pubblicazioni/rapporti\\_eventi/2016/REM\\_20161121-25%20AllertaRossa\\_vers20170217.pdf](http://www.arpal.liguria.it/contenuti_statici/pubblicazioni/rapporti_eventi/2016/REM_20161121-25%20AllertaRossa_vers20170217.pdf).

784

785 ARPA Piemonte, 2017: Gli eventi alluvionali in piemonte - evento del 21-25 novembre 2016. Tech.  
786 rep. URL <http://www.arpa.piemonte.it/pubblicazioni-2/gli-eventi-alluvionali-in-piemonte>.

787 Auffhammer, M., P. Baylis, and C. H. Hausman, 2017: Climate change is projected to have severe  
788 impacts on the frequency and intensity of peak electricity demand across the united states.  
789 *Proceedings of the National Academy of Sciences*, **114** (8), 1886–1891.

790 Bauer, P., A. Thorpe, and G. Brunet, 2015: The quiet revolution of numerical weather prediction.  
791 *Nature*, **525** (7567), 47–55.

792 Bayr, T., D. I. V. Domeisen, and C. Wengel, 2019: The effect of the equatorial Pacific cold SST  
793 bias on simulated ENSO teleconnections to the North Pacific and California. *Climate Dynamics*,  
794 **31** (1), 1–19.

795 Beerli, R., H. Wernli, and C. M. Grams, 2017: Does the lower stratosphere provide predictabil-  
796 ity for month-ahead wind electricity generation in Europe? *Quarterly Journal of the Royal*  
797 *Meteorological Society*, **143** (709), 3025–3036.

798 Bendix, J., K. Trachte, J. Cermak, R. Rollenbeck, and T. Nauß, 2009: Formation of Convective  
799 Clouds at the Foothills of the Tropical Eastern Andes (South Ecuador). *Journal of Applied*  
800 *Meteorology and Climatology*, **48** (8), 1682–1695.

801 Berg, A., and J. Sheffield, 2018: Climate Change and Drought: the Soil Moisture Perspective.  
802 *Current Climate Change Reports*, **4** (2), 180–191.

803 Bloomfield, H., D. J. Brayshaw, L. Shaffrey, P. J. Coker, and H. E. Thornton, 2018: The changing  
804 sensitivity of power systems to meteorological drivers: a case study of great britain. *Environmental*  
805 *Research Letters*, **13 (5)**, 054 028.

806 Bloomfield, H., C. Suitters, and D. Drew, 2020: Meteorological drivers of European power system  
807 stress. *Journal of Renewable Energy*, **2020 (5481010)**.

808 Brás, T. A., J. Seixas, N. Carvalhais, and J. Jägermeyr, 2021: Severity of drought and heatwave  
809 crop losses tripled over the last five decades in Europe. *Environmental Research Letters*.

810 Brunner, L., N. Schaller, J. Anstey, J. Sillmann, and A. K. Steiner, 2018: Dependence of Present and  
811 Future European Temperature Extremes on the Location of Atmospheric Blocking. *Geophysical*  
812 *Research Letters*, **45 (12)**, 6311–6320.

813 Buizza, R., and Coauthors, 2017: IFS Cycle 43r3 brings model and assimilation updates. *ECMWF*  
814 *Newsletter*, **152**, 18–22.

815 Bunzel, F., W. A. Mueller, M. Dobrynin, K. Froehlich, S. Hagemann, H. Pohlmann, T. Stacke, and  
816 J. Baehr, 2018: Improved Seasonal Prediction of European Summer Temperatures With New  
817 Five-Layer Soil-Hydrology Scheme. *Geophysical Research Letters*, **45 (1)**, 346–353.

818 Bureau of Meteorology, 2019: Special Climate Statement 69 — an Extended Period of Heavy  
819 Rainfall and Flooding in Tropical Queensland.

820 Buzzi, A., S. Davolio, P. Malguzzi, O. Drofa, and D. Mastrangelo, 2014: Heavy rainfall episodes  
821 over Liguria in autumn 2011: numerical forecasting experiments. *Natural Hazards and Earth*  
822 *System Sciences*, **14 (5)**, 1325–1340, doi:10.5194/nhess-14-1325-2014.

823 Camargo, S., and S. Hsiang, 2015: Chapter 18: Tropical Cyclones: From the influence of climate  
824 to their socio-economic impacts. *Extreme Events: Observations, Modeling and Economics*,

825 M. G. M. Chaves, and J. Urrutia-Fucugauchi, Eds., AGU Monograph, Wiley-Blackwell, ISBN:  
826 978-1-119-15701-4, 303–342, doi:10.1002/9781119157052.ch18.

827 Camargo, S. J., 2016: Western North Pacific Basin, in "State of the Climate in 2015". *Bull. Amer.*  
828 *Meteor. Soc.*, **97**, S110–S113.

829 Camargo, S. J., F. Vitart, C.-Y. Lee, and M. K. Tippett, 2021: Skill, predictability, and cluster  
830 analysis of Atlantic tropical storms and hurricanes in the ECMWF monthly forecasts. *Monthly*  
831 *Weather Review*, doi:10.1175/MWR-D-21-0075.1.

832 Camargo, S. J., M. C. Wheeler, and A. H. Sobel, 2009: Diagnosis of the MJO modulation of  
833 tropical cyclogenesis using an empirical index. *J. Atmos. Sci.*, **66**, 3061–3074.

834 Camargo, S. J., and Coauthors, 2019: Tropical cyclone prediction on subseasonal time-scales.  
835 *Trop. Cyclone Res. Rev.*, **8**, 150–165, doi:10.1038/j.tccr.2019.10.004.

836 Camp, J., and Coauthors, 2018: Skilful multi-week tropical cyclone prediction in ACCESS-S1 and  
837 the role of the MJO. *Q. J. R. Meteorol. Soc.*, **144**, 1337–1351, doi:10.1002/qj.3260.

838 Campbell, S., T. A. Remenyi, C. J. White, and F. H. Johnston, 2018: Heatwave and health impact  
839 research: A global review. *Health & place*, **53**, 210–218.

840 Carrera, M. L., R. W. Higgins, and V. E. Kousky, 2004: Downstream Weather Impacts Associated  
841 with Atmospheric Blocking over the Northeast Pacific. *Journal of Climate*, **17 (24)**, 4823–4839.

842 Cavicchia, L., H. von Storch, and S. Gualdi, 2014: A long-term climatology of medicane. *Clim.*  
843 *Dyn.*, **43**, 1183–1195, doi:10.1007/s00382-013-1893-7.

844 CEPAL, 2018: ECLAC team assesses impact of Volcán de Fuego eruption in Guatemala. Tech.  
845 Rep. 8, 6 pp.

846 Chand, S. S., and Coauthors, 2019: Review of tropical cyclones in the Australian region: Climatology, variability, predictability and trends. *WIREs Clim. Change*, **10**, e602, doi:10.1002/wcc602.

847

848 Charlton-Perez, A. J., R. W. Aldridge, C. M. Grams, and R. Lee, 2019: Winter pressures on the

849 UK health system dominated by the Greenland Blocking weather regime. *Weather and Climate*

850 *Extremes*, **25**, 100 218.

851 Charlton-Perez, A. J., L. Ferranti, and R. W. Lee, 2018: The influence of the stratospheric state

852 on North Atlantic weather regimes. *Quarterly Journal of the Royal Meteorological Society*,

853 **144 (713)**, 1140–1151.

854 Charlton-Perez, A. J., W. T. K. Huang, and S. H. Lee, 2021: Impact of sudden stratospheric

855 warmings on United Kingdom mortality. *Atmospheric Science Letters*, **22 (2)**, e1013.

856 Chen, M., W. Shi, P. Xie, V. B. Silva, V. E. Kousky, R. Wayne Higgins, and J. E. Janowiak, 2008:

857 Assessing objective techniques for gauge-based analyses of global daily precipitation. *Journal*

858 *of Geophysical Research: Atmospheres*, **113 (D4)**.

859 Coelho, C. A., B. Brown, L. Wilson, M. Mittermaier, and B. Casati, 2019: Forecast verification

860 for s2s timescales. *Sub-Seasonal to Seasonal Prediction*, Elsevier, 337–361.

861 Coelho, C. A., M. A. Firpo, F. M. de Andrade, and Coauthors, 2018: A verification framework

862 for south american sub-seasonal precipitation predictions. *Meteorologische Zeitschrift*, **27 (6)**,

863 503–520.

864 Cohen, J., and J. Jones, 2011: A new index for more accurate winter predictions. *Geophysical*

865 *Research Letters*, **38 (21)**, L21 701.

866 CONRED, 2018: Informe Erupción Volcán de Fuego. Tech. rep. URL [https://conred.gob.gt/site/informacion\\_publica/gobierno\\_abierto20162018/Meta4\\_Agosto2018.pdf](https://conred.gob.gt/site/informacion_publica/gobierno_abierto20162018/Meta4_Agosto2018.pdf), Downloaded on April 1st, 2020.

869 Cowan, T., and Coauthors, 2019: Forecasting the extreme rainfall, low temperatures, and strong  
870 winds associated with the northern Queensland floods of February 2019. *Weather and Climate  
871 Extremes*, **26**, 100 232.

872 Cradden, L. C., and F. McDermott, 2018: A weather regime characterisation of irish wind gen-  
873 eration and electricity demand in winters 2009–11. *Environmental Research Letters*, **13 (5)**,  
874 054 022.

875 Cremonini, R., and D. Tiranti, 2018: The Weather Radar Observations Applied to Shallow  
876 Landslides Prediction: A Case Study From North-Western Italy. *Frontiers in Earth Science*,  
877 **6**, 134, doi:10.3389/feart.2018.00134, URL <https://www.frontiersin.org/article/10.3389/feart.2018.00134>.

879 Davies, R., 2016: Ecuador – 1 dead after floods and landslides – 14cm of rain in 24 hours in esmer-  
880 aldas. Tech. rep. URL <http://floodlist.com/america/ecuador-floods-esmeraldas-january-2016>.

881 Davolio, S., P. Malguzzi, O. Drofa, D. Mastrangelo, and A. Buzzi, 2020: The Piedmont flood  
882 of November 1994: a testbed of forecasting capabilities of the CNR-ISAC meteorological  
883 model suite. *Bulletin of Atmospheric Science and Technology*, **1 (3)**, 263–282, doi:10.1007/s42865-020-00015-4.

885 de Andrade, F. M., C. A. S. Coelho, and I. F. A. Cavalcanti, 2019: Global precipitation hindcast  
886 quality assessment of the Subseasonal to Seasonal (S2S) prediction project models. *Climate  
887 Dynamics*, **52 (9)**, 5451–5475.

888 de Vries, H., R. J. Haarsma, and W. Hazeleger, 2012: Western European cold spells in current and  
889 future climate. *Geophysical Research Letters*, **39** (4), doi:10.1029/2011GL050665.

890 DeFlorio, M. J., and Coauthors, 2019: Experimental Subseasonal-to-Seasonal (S2S) Forecasting  
891 of Atmospheric Rivers Over the Western United States. *Journal of Geophysical Research-  
892 Atmospheres*, **124** (21), 11 242–11 265.

893 Deloitte, 2019: The social and economic cost of the North and Far North Queensland  
894 Monsoon Trough. URL [https://www2.deloitte.com/au/en/pages/economics/articles/  
895 social-economic-cost-north-far-north-queensland-monsoon-trough.html](https://www2.deloitte.com/au/en/pages/economics/articles/social-economic-cost-north-far-north-queensland-monsoon-trough.html).

896 DeMott, C., Á. G. Muñoz., C. Roberts, C. Spillman, and F. Vitart, 2021: The Benefits of Better  
897 Ocean Weather Forecasting. *Eos*, **102**, doi:10.1029/2021eo210601.

898 Ding, Q., and B. Wang, 2005: Circumglobal teleconnection in the Northern Hemisphere summer.  
899 *Journal of Climate*, **18** (17), 3483–3505.

900 Dirmeyer, P. A., and Coauthors, 2018: Verification of land-atmosphere coupling in forecast models,  
901 reanalyses and land surface models using flux site observations. *Journal of Hydrometeorology*,  
902 **19** (No 2), 375–392.

903 DiSera, L., H. Sjödin, J. Rocklöv, Y. Tozan, B. Súdre, H. Zeller, and Á. G. Muñoz,  
904 2020: The Mosquito, the Virus, the Climate: An Unforeseen Réunion in 2018. *Geo-  
905 Health*, **4** (8), doi:10.1029/2020GH000253, URL <https://onlinelibrary.wiley.com/doi/abs/10.1029/2020GH000253>.

906 Dittmann, E., P. Hechler, and P. Bissolli, 2004: Annual Bulletin on the Climate in WMO Region  
907 VI - 2003. Tech. rep. URL [https://www.dwd.de/DE/leistungen/ravibulletinjahr/archiv/bulletin\\_2003.pdf?\\_\\_blob=publicationFile&v=4](https://www.dwd.de/DE/leistungen/ravibulletinjahr/archiv/bulletin_2003.pdf?__blob=publicationFile&v=4).

910 Dobrynin, M., and Coauthors, 2018: Improved Teleconnection-Based Dynamical Seasonal Pre-  
911 dictions of Boreal Winter. *Geophysical Research Letters*, **44** (9-10), 2723.

912 Domeisen, D. I. V., 2019: Estimating the Frequency of Sudden Stratospheric Warming Events  
913 From Surface Observations of the North Atlantic Oscillation. *Journal of Geophysical Research-  
914 Atmospheres*, **124** (6), 3180–3194.

915 Domeisen, D. I. V., and A. H. Butler, 2020: Stratospheric drivers of extreme events at the Earth's  
916 surface. *Communications Earth & Environment*, 1–8.

917 Domeisen, D. I. V., A. H. Butler, K. Fröhlich, M. Bittner, W. Müller, and J. Baehr, 2015: Seasonal  
918 predictability over Europe arising from El Niño and stratospheric variability in the MPI-ESM  
919 Seasonal Prediction System. *Journal of Climate*, **28** (1), 256–271.

920 Domeisen, D. I. V., and Coauthors, 2020a: The Role of the Stratosphere in Subseasonal to Seasonal  
921 Prediction: 1. Predictability of the Stratosphere. *Journal of Geophysical Research-Atmospheres*,  
922 **125** (2), 1–17.

923 Domeisen, D. I. V., and Coauthors, 2020b: The Role of the Stratosphere in Subseasonal to  
924 Seasonal Prediction: 2. Predictability Arising From Stratosphere-Troposphere Coupling. *Journal  
925 of Geophysical Research-Atmospheres*, **125** (2), 1–20.

926 Donat, M. G., A. L. Lowry, L. V. Alexander, P. A. O'Gorman, and N. Maher, 2016: More extreme  
927 precipitation in the world's dry and wet regions. *Nature Climate Change*, **6** (5), 508–513.

928 Dong, L., C. Mitra, S. Greer, and E. Burt, 2018: The Dynamical Linkage of Atmospheric Blocking  
929 to Drought, Heatwave and Urban Heat Island in Southeastern US: A Multi-Scale Case Study.  
930 *Atmosphere*, **9** (1), 33.

931 Dorninger, M., E. Gilleland, B. Casati, M. P. Mittermaier, E. E. Ebert, B. G. Brown, and L. J.  
932 Wilson, 2018: The Setup of the MesoVICT Project. *Bulletin of the American Meteorological*  
933 *Society*, **99** (9), 1887–1906.

934 Dorrington, J., I. Finney, T. Palmer, and A. Weisheimer, 2020: Beyond skill scores: exploring  
935 sub-seasonal forecast value through a case-study of French month-ahead energy prediction.  
936 *Quarterly Journal of the Royal Meteorological Society*, **146** (733), 3623–3637.

937 Doss-Gollin, J., D. J. Farnham, U. Lall, and V. Modi, 2021: How unprecedented was the february  
938 2021 texas cold snap? *Environmental Research Letters*, **16** (6), 064 056, doi:10.1088/1748-9326/  
939 ac0278, URL <https://doi.org/10.1088/1748-9326/ac0278>.

940 Doss-Gollin, J., Á. G. Muñoz, S. J. Mason, and M. Pastén, 2018: Heavy Rainfall in Paraguay during  
941 the 2015/16 Austral Summer: Causes and Subseasonal-to-Seasonal Predictive Skill. *Journal of*  
942 *Climate*, **31** (17), 6669–6685.

943 Duan, H., S. Wang, and J. Feng, 2013: The national drought situation and its impacts and causes  
944 in the summer 2013. *Journal of Arid Meteorology*, **31** (3), 633–640.

945 Duchez, A., and Coauthors, 2016: Drivers of exceptionally cold North Atlantic Ocean temperatures  
946 and their link to the 2015 European heat wave. *Environmental Research Letters*, **11** (7), 1–9.

947 ECMWF, 2019: ECMWF - Severe Event Catalogue - 2018 - 201809 Rainfall Zorbas. URL  
948 <https://confluence.ecmwf.int/display/FCST/201809+-+Rainfall+-+Zorbas#app-switcher>.

949 Emanuel, K., F. Fondriest, and J. Kossin, 2012: Potential Economic Value of Seasonal Hurricane  
950 Forecasts. *Weather, Climate, and Society*, **4** (2), 110–117.

951 Emerton, R., and Coauthors, 2020: Emergency flood bulletins for Cyclones Idai and Kenneth: A  
952 critical evaluation of the use of global flood forecasts for international humanitarian preparedness  
953 and response. *International Journal of Disaster Risk Reduction*, **50**, 101 811.

954 Enomoto, T., 2004: Interannual variability of the Bonin high associated with the propagation of  
955 Rossby waves along the Asian jet. *Journal of the Meteorological Society of Japan. Ser. II*, **82** (4),  
956 1019–1034.

957 Evans, J. L., and R. J. Allan, 1992: El Niño/Southern Oscillation modification to the structure of  
958 the monsoon and tropical cyclone activity in the Australian region. *Int. J. Climatol.*, **12**, 611–623.

959 Ferranti, L., L. Magnusson, F. Vitart, and D. S. Richardson, 2018: How far in advance can we  
960 predict changes in large-scale flow leading to severe cold conditions over europe? *Quarterly  
961 Journal of the Royal Meteorological Society*, **144** (715), 1788–1802.

962 Ferranti, L., L. Magnusson, F. Vitart, and D. S. Richardson, 2019: A new product to flag up the  
963 risk of cold spells in Europe weeks ahead. *ECMWF Newsletter*, **158**, 15–20.

964 Ferranti, L., and P. Viterbo, 2006: The European Summer of 2003: Sensitivity to Soil Water Initial  
965 Conditions. *Journal of Climate*, **19** (15), 3659–3680.

966 Fischer, E. M., S. I. Seneviratne, P. L. Vidale, D. Lüthi, and C. Schär, 2007: Soil Moisture-  
967 Atmosphere Interactions during the 2003 European Summer Heat Wave. *J. Atmos. Sci.*, **20**,  
968 5081–5099.

969 Flaounas, E., S. L. Gray, and F. Teubler, 2021: A process-based anatomy of Mediterranean  
970 cyclones: from baroclinic lows to tropical-like systems. *Weather and Climate Dynamics*, **2** (1),  
971 255–279.

972 Flaounas, E., S. Raveh-Rubin, H. Wernli, P. D. C. Dynamics, and N. Butchart, 2015: The dynamical  
973 structure of intense Mediterranean cyclones. *Climate Dynamics*.

974 Ford, T. W., P. A. Dirmeyer, and D. O. Benson, 2018: Evaluation of heat wave forecasts seamlessly  
975 across subseasonal timescales. *NPJ Climate and Atmospheric Science*, **1** (1), 1–9.

976 Fragkoulidis, G., V. Wirth, P. Bossmann, and A. H. Fink, 2018: Linking Northern Hemisphere  
977 temperature extremes to Rossby wave packets. *Quarterly Journal of the Royal Meteorological  
978 Society*, **144** (711), 553–566.

979 Freychet, N., S. Tett, J. Wang, and G. Hegerl, 2017: Summer heat waves over eastern China:  
980 Dynamical processes and trend attribution. *Environmental Research Letters*, **12** (2), 024 015.

981 Gao, M., B. Wang, J. Yang, and W. Dong, 2018: Are Peak Summer Sultry Heat Wave Days  
982 over the Yangtze–Huaihe River Basin Predictable? *Journal of Climate*, **36** (6), 2185–2196,  
983 doi:10.1175/JCLI-D-17-0342.1.

984 García-Herrera, R., and Coauthors, 2019: The European 2016/17 Drought. *Journal of Climate*,  
985 **32** (11), 3169 – 3187, doi:10.1175/JCLI-D-18-0331.1.

986 Gershunov, A., 1998: ENSO Influence on Intraseasonal Extreme Rainfall and Temperature Fre-  
987 quencies in the Contiguous United States: Implications for Long-Range Predictability. *Journal  
988 of Climate*, **11** (12), 3192–3203.

989 Gershunov, A., and K. Guirguis, 2012: California heat waves in the present and future. *Geophysical  
990 Research Letters*, **39** (18).

991 Gershunov, A., and K. Guirguis, 2015: California heat waves, july 2015. Tech. rep. URL <https://www.swcasc.arizona.edu/sites/default/files/HeatWaves.pdf>.

993 Goddard, L., W. E. Baethgen, H. Bhojwani, and A. W. Robertson, 2014: The International  
994 Research Institute for Climate & Society: why, what and how. *Earth Perspectives*, **1** (1), 10,  
995 doi:10.1186/2194-6434-1-10.

996 Goddard, L., and Coauthors, 2020: Climate Services Ecosystems in times of COVID-19. *WMO*  
997 *at 70 - Responding to a Global Pandemic*. *WMO Bulletin* 69(2), **69** (2), 39–46, URL <https://public.wmo.int/en/resources/bulletin/climate-services-ecosystems-times-of-covid-19>  
998 <https://hdl.handle.net/10568/111389>.

1000 Grazzini, F., and F. Vitart, 2015: Atmospheric predictability and Rossby wave packets. *Quarterly*  
1001 *Journal of the Royal Meteorological Society*, **141** (692), 2793–2802.

1002 Gregory, P. A., J. Camp, K. Bigelow, and A. Brown, 2019: Sub-seasonal predictability of the  
1003 2017–2018 southern hemisphere tropical cyclone season. *Atmos. Sci. Lett.*, **20**, e886, doi:10.  
1004 1002/asl.886.

1005 Gruber, K., T. Gauster, L. Ramirez-Camargo, G. Laaha, and J. Schmidt, 2021: The Texas 2021  
1006 cold spell in a climate-power system perspective. doi:10.5194/egusphere-egu21-7180, URL  
1007 <https://doi.org/10.5194/egusphere-egu21-7180>.

1008 Hall, J. D., A. J. Matthews, and D. J. Karoli, 2001: The modulation of tropical cyclone activity in  
1009 the Australian region by the Madden-Julian Oscillation. *Mon. Wea. Rev.*, **129**, 2970–2982.

1010 Hamill, T. M., and G. N. Kiladis, 2014: Skill of the MJO and Northern Hemisphere Blocking in  
1011 GEFS Medium-Range Reforecasts. *Monthly Weather Review*, **142** (2), 868–885.

1012 Hartmann, D. L., 2015: Pacific sea surface temperature and the winter of 2014. *Geophysical*  
1013 *Research Letters*, **42** (6), 1894–1902.

1014 Hauser, M., R. Orth, and S. I. Seneviratne, 2016: Role of soil moisture versus recent climate change  
1015 for the 2010 heat wave in western Russia. *Geophysical Research Letters*, **43** (6), 2819–2826.

1016 Hersbach, H., and Coauthors, 2020: The ERA5 Global Reanalysis. *Quarterly Journal of the Royal*  
1017 *Meteorological Society*, qj.3803, doi:10.1002/qj.3803, URL <https://onlinelibrary.wiley.com/doi/abs/10.1002/qj.3803>.

1019 Hsiang, S., 2010: Temperatures and cyclones strongly associated with economic production in the  
1020 Caribbean and Central America. *Proceedings of the National Academy of Sciences*, **107** (35).

1021 Hsiang, S., and D. Narita, 2012: Adaptation to cyclone risk: Evidence from the global cross-  
1022 section. *Climate Change Economics*, **03** (02), 1250 011, doi:10.1142/S201000781250011X.

1023 Huang, W., and X. Liang, 2010: Convective asymmetries associated with tropical cyclone  
1024 landfall:  $\beta$ -plane simulations. *Advances in Atmospheric Sciences*, **27** (4), 795–806, doi:  
1025 10.1007/s00376-009-9086-3.

1026 IRI, 2018: Adapting Agriculture to Climate Today, for Tomorrow (ACToday), a Columbia World  
1027 Project. Tech. rep. URL <https://iri.columbia.edu/actoday>.

1028 Janiga, M., C. J. Schreck, J. A. Ridout, M. Flatau, N. P. Barton, E. J. Metzger, and C. A. Reynolds,  
1029 2018: Subseasonal forecasts of convectively coupled equatorial waves and the MJO: Activity  
1030 and predictive skill. *Mon. Wea. Rev.*, **146**, 2337–2360, doi:10.1175/MWR-D-17-0261.1.

1031 Jian-Qi, S., 2012: Possible impact of the summer North Atlantic Oscillation on extreme hot events  
1032 in China. *Atmospheric and Oceanic Science Letters*, **5** (3), 231–234.

1033 Jing-Bei, P., 2014: An investigation of the formation of the heat wave in southern China in summer  
1034 2013 and the relevant abnormal subtropical high activities. *Atmospheric and Oceanic Science*  
1035 *Letters*, **7** (4), 286–290.

1036 JMA, 2013: Extreme summer conditions in Japan in 2013. *Tokyo Climate Center, Japan Meteorological Agency*, 9pp, URL [https://ds.data.jma.go.jp/tcc/tcc/news/press\\_20130902.pdf](https://ds.data.jma.go.jp/tcc/tcc/news/press_20130902.pdf).

1037

1038 Jones, C., D. E. Waliser, K. M. Lau, and W. Stern, 2004: Global Occurrences of Extreme  
1039 Precipitation and the Madden–Julian Oscillation: Observations and Predictability. *Journal of*  
1040 *Climate*, **17 (23)**, 4575–4589, doi:10.1175/3238.1.

1041 Jones, D. A., W. Wang, and R. Fawcett, 2009: High-quality spatial climate data-sets for Australia.  
1042 *Australian Meteorological and Oceanographic Journal*, **58 (4)**, 233.

1043 Karpechko, A. Y., A. Charlton-Perez, M. Balmaseda, N. Tyrrell, and F. Vitart, 2018: Predicting  
1044 Sudden Stratospheric Warming 2018 and Its Climate Impacts With a Multimodel Ensemble.  
1045 *Geophysical Research Letters*, **45 (24)**, 13,538–13,546, doi:10.1029/2018GL081091.

1046 Kautz, L.-A., I. Polichtchouk, T. Birner, H. Garny, and J. G. Pinto, 2020: Enhanced extended-  
1047 range predictability of the 2018 late-winter eurasian cold spell due to the stratosphere. *Quarterly*  
1048 *Journal of the Royal Meteorological Society*, **146 (727)**, 1040–1055, doi:10.1002/qj.3724.

1049 Kenyon, J., and G. C. Hegerl, 2010: Influence of Modes of Climate Variability on Global Precipi-  
1050 tation Extremes. *Journal of Climate*, **23**, 6248–6262, doi:10.1175/2010JCLI3617.1.

1051 Khodayar, S., N. Kalthoff, and C. Kottmeier, 2018: Atmospheric conditions associated with heavy  
1052 precipitation events in comparison to seasonal means in the western mediterranean region.  
1053 *Climate Dynamics*, **51 (3)**, 951–967, doi:10.1007/s00382-016-3058-y.

1054 Kiladis, G. N., J. Dias, K. H. Straub, M. C. Wheeler, S. N. Tulich, K. Kikuchi, K. M. Weickmann,  
1055 and M. J. Ventrice, 2014: A comparison of OLR and circulation-based indices for tracking the  
1056 MJO. *Mon. Wea. Rev.*, **142**, 1697–1715, doi:10.1175/MWR-D-13-00301.1.

1057 Kim, Y.-H., S.-K. Min, D. A. Stone, H. Shiogama, and P. Wolski, 2018: Multi-model event  
1058 attribution of the summer 2013 heat wave in Korea. *Weather and climate extremes*, **20**, 33–44.

1059 King, A. D., D. Hudson, E.-P. Lim, A. G. Marshall, H. H. Hendon, T. P. Lane, and O. Alves, 2020:  
1060 Sub-seasonal to seasonal prediction of rainfall extremes in Australia. *Quarterly Journal of the*  
1061 *Royal Meteorological Society*, 1–22, doi:10.1002/qj.3789.

1062 King, A. D., N. P. Klingaman, L. V. Alexander, M. G. Donat, N. C. Jourdain, and P. Maher,  
1063 2014: Extreme Rainfall Variability in Australia: Patterns, Drivers, and Predictability. *Journal*  
1064 *of Climate*, **27 (15)**, 6035–6050, doi:10.1175/JCLI-D-13-00715.1.

1065 Knapp, K. R., M. C. Kruk, D. H. Levinson, H. J. Diamond, and C. J. Neumann, 2010: The  
1066 international best track archive for climate stewardship (IBTrACS) unifying tropical cyclone data.  
1067 *Bulletin of the American Meteorological Society*, **91 (3)**, 363–376, doi:10.1175/2009BAMS2755.  
1068 1.

1069 Knight, J., and Coauthors, 2021: Predictability of european winters 2017/2018 and 2018/2019:  
1070 Contrasting influences from the tropics and stratosphere. *Atmospheric Science Letters*, **22 (1)**,  
1071 e1009.

1072 Knutson, T., and Coauthors, 2019: Tropical cyclones and climate change assessment: Part I. Detec-  
1073 tion and attribution. *Bull. Amer. Meteor. Soc.*, **100**, 1987–2007, doi:10.1175/BAMS-D-18-0189.  
1074 1.

1075 Knutson, T., and Coauthors, 2020: Tropical cyclones and climate change assessment: Part II.  
1076 Projected response to anthropogenic warming. *Bull. Amer. Meteor. Soc.*, **101**, E303–E322, doi:  
1077 10.1175/BAMS-D-18-0194.1.

1078 Kolstad, E. W., 2021: Prediction and precursors of Idai and 38 other tropical cyclones and storms  
1079 in the Mozambique Channel. *Quarterly Journal of the Royal Meteorological Society*, **147** (734),  
1080 45–57, doi:<https://doi.org/10.1002/qj.3903>.

1081 Kolstad, E. W., T. J. Bracegirdle, and I. A. Seierstad, 2009: Marine cold-air outbreaks in the  
1082 north atlantic: Temporal distribution and associations with large-scale atmospheric circulation.  
1083 *Climate dynamics*, **33** (2-3), 187–197.

1084 Kolstad, E. W., T. Breiteig, and A. A. Scaife, 2010: The association between stratospheric weak  
1085 polar vortex events and cold air outbreaks in the northern hemisphere. *Quarterly Journal of the*  
1086 *Royal Meteorological Society*, **136** (649), 886–893.

1087 Kornhuber, K., S. Osprey, D. Coumou, S. Petri, V. Petoukhov, S. Rahmstorf, and L. Gray, 2019:  
1088 Extreme weather events in early summer 2018 connected by a recurrent hemispheric wave-7  
1089 pattern. *Environmental Research Letters*, **14** (5), 054002–8.

1090 Koster, R. D., and Coauthors, 2010: Contribution of land surface initialization to subseasonal  
1091 forecast skill: First results from a multi-model experiment. *Geophysical Research Letters*, **37** (2).

1092 Kueh, M.-T., and C.-Y. Lin, 2020: The 2018 summer heatwaves over northwestern europe and its  
1093 extended-range prediction. *Scientific reports*, **10** (1), 1–18.

1094 Landgren, O. A., I. A. Seierstad, and T. Iversen, 2019: Projected future changes in marine cold-air  
1095 outbreaks associated with polar lows in the northern north-atlantic ocean. *Climate Dynamics*,  
1096 **53** (5), 2573–2585.

1097 Lee, C.-Y., S. J. Camargo, F. Vitart, A. H. Sobel, J. Camp, S. Wang, M. K. Tippett, and Q. Yang,  
1098 2020: Subseasonal predictions of tropical cyclone occurrence and ACE in the S2S dataset. *Wea.*  
1099 *Forecasting*, **35**, 921–938, doi:10.1175/WAF-D-19-0217.1.

1100 Lee, C.-Y., S. J. Camargo, F. Vitart, A. H. Sobel, and M. K. Tippett, 2018: Subseasonal tropical  
1101 cyclone genesis prediction and MJO in the S2S dataset. *Wea. Forecasting*, **33**, 967–988, doi:  
1102 10.1175/WAF-D-17-0165.1.

1103 Lee, M., and T. Frisius, 2018: On the role of convective available potential energy (CAPE) in  
1104 tropical cyclone intensification. *Tellus A: Dynamic Meteorology and Oceanography*, **70** (1),  
1105 1–18, doi:10.1080/16000870.2018.1433433.

1106 Lehtonen, I., and A. Y. Karpechko, 2016: Observed and modeled tropospheric cold anomalies  
1107 associated with sudden stratospheric warmings. *Journal of Geophysical Research: Atmospheres*,  
1108 **121** (4), 1591–1610, doi:10.1002/2015JD023860.

1109 Lenggenhager, S., and O. Martius, 2019: Atmospheric blocks modulate the odds of heavy precipi-  
1110 tation events in Europe. *Climate Dynamics*, **53**, 4155–4171, doi:10.1007/s00382-019-04779-0.

1111 Leroy, A., and M. C. Wheeler, 2008: Statistical prediction of weekly tropical cyclone activity in  
1112 the southern hemisphere. *Mon. Wea. Rev.*, **136**, 3637–3654.

1113 Levinson, D., and A. Waple, 2004: State of the climate in 2003. *Bulletin of the American Meteo-*  
1114 *rological society*, **85** (6), S1–S72.

1115 Li, J., T. Ding, X. Jia, and X. Zhao, 2015: Analysis on the extreme heat wave over China around  
1116 Yangtze River region in the summer of 2013 and its main contributing factors. *Advances in*  
1117 *Meteorology*, **2015**.

1118 Li, M., Y. Yao, D. Luo, and L. Zhong, 2019: The linkage of the large-scale circulation pattern to a  
1119 long-lived heatwave over Mideastern China in 2018. *Atmosphere*, **10** (2), 89.

1120 Li, Y., D. Tian, and H. Medina, 2021: Multimodel Subseasonal Precipitation Forecasts over  
1121 the Contiguous United States: Skill Assessment and Statistical Postprocessing. *Journal of*  
1122 *Hydrometeorology*, **22** (10), 2581–2600.

1123 Li, Chao, Zwiers, Francis, Zhang, Xuebin, Li, Guilong, Sun, Ying, and Wehner, Michael, 2021:  
1124 Changes in Annual Extremes of Daily Temperature and Precipitation in CMIP6 Models. *Journal*  
1125 *of Climate*, **34** (9), 3441–3460.

1126 Liberto, T. D., 2019: Heat wave broils the U.S. Southeast over Memorial  
1127 Day weekend 2019. URL [https://www.climate.gov/news-features/event-tracker/](https://www.climate.gov/news-features/event-tracker/heat-wave-broils-us-southeast-over-memorial-day-weekend-2019)  
1128 [heat-wave-broils-us-southeast-over-memorial-day-weekend-2019](https://www.climate.gov/news-features/event-tracker/heat-wave-broils-us-southeast-over-memorial-day-weekend-2019).

1129 Lin, I.-I., and Coauthors, 2017: *El Niño Southern Oscillation in a Changing Climate*, chap. ENSO  
1130 and Tropical Cyclones, 377–408. Geophysical Monograph Series, American Geophysical Union,  
1131 Wiley.

1132 Liu, X., B. He, L. Guo, L. Huang, and D. Chen, 2020: Similarities and Differences in the  
1133 Mechanisms Causing the European Summer Heatwaves in 2003, 2010, and 2018. *Earth's Future*,  
1134 **8** (4), e2019EF001386.

1135 Lopez, H., R. West, S. Dong, G. Goni, B. Kirtman, S.-K. Lee, and R. Atlas, 2018: Early emergence  
1136 of anthropogenically forced heat waves in the western United States and Great Lakes. *Nature*  
1137 *Climate Change*, **8** (5), 414–420.

1138 Luo, L., and Y. Zhang, 2012: Did we see the 2011 summer heat wave coming? *Geophysical*  
1139 *Research Letters*, **39** (9).

1140 Magnusson, L., 2017: 151. The cold spell in eastern Europe in January 2017. URL <https://www.ecmwf.int/en/newsletter/151/news/cold-spell-eastern-europe-january-2017>, 22–27 pp.

1142 Maidens, A., A. Arribas, A. A. Scaife, C. MacLachlan, D. Peterson, and J. Knight, 2013: The  
1143 influence of surface forcings on prediction of the north atlantic oscillation regime of winter  
1144 2010/11. *Monthly Weather Review*, **141** (11), 3801–3813.

1145 Manrique-Suñén, A., N. Gonzalez-Reviriego, V. Torralba, N. Cortesi, and F. J. Doblas-  
1146 Reyes, 2020: Choices in the verification of S2S forecasts and their implica-  
1147 tions for climate services. *Monthly Weather Review*, **148** (10), 3995–4008, doi:10.  
1148 1175/MWR-D-20-0067.1, URL <https://journals.ametsoc.org/mwr/article/148/10/3995/353477/Choices-in-the-Verification-of-S2S-Forecasts-and>.

1150 Manzanas, R., J. M. Gutiérrez, J. Bhend, S. Hemri, F. J. Doblas-Reyes, V. Torralba, E. Penabad,  
1151 and A. Brookshaw, 2019: Bias adjustment and ensemble recalibration methods for seasonal  
1152 forecasting: a comprehensive intercomparison using the C3S dataset. *Clim. Dyn.*, doi:10.1007/  
1153 s00382-019-04640-4.

1154 Mason, S., M. K. Tippet, L. Song, and A. G. M. noz, 2021: Climate Predictability Tool  
1155 v17.4.4. Columbia University Academic Commons. Tech. rep. doi:<https://doi.org/10.7916/d8-1bcm-8620>.

1157 Materia, S., Á. G. Muñoz, M. C. Álvarez-Castro, S. J. Mason, F. Vitart, and S. Gualdi, 2020a: Mul-  
1158 timodel subseasonal forecasts of spring cold spells: Potential value for the hazelnut agribusiness.  
1159 *Weather and Forecasting*, **35** (1), 237–254.

1160 Materia, S., Á. G. Muñoz, M. C. Alvarez-Castro, S. J. Mason, F. Vitart, and S. Gualdi, 2020b:  
1161 Multimodel Subseasonal Forecasts of Spring Cold Spells: Potential Value for the Hazelnut  
1162 Agribusiness. *Weather and Forecasting*, **35** (1), 237–254.

1163 McKinnon, K. A., A. Rhines, M. P. Tingley, and P. Huybers, 2016: Long-lead predictions of  
1164 eastern United States hot days from Pacific sea surface temperatures. *Nature Geoscience*, **9** (5),  
1165 389–394.

1166 Merryfield, W. J., and Coauthors, 2020: Current and Emerging Developments in Subseasonal to  
1167 Decadal Prediction. *Bulletin of the American Meteorological Society*, **101** (6), E869–E896.

1168 Merz, B., and Coauthors, 2020: Impact Forecasting to Support Emergency Management of Natural  
1169 Hazards. *Reviews of Geophysics*, doi:10.1029/2020RG000704.

1170 Miglietta, M. M., D. Cerrai, S. Laviola, E. Cattani, and V. Levizzani, 2017: Potential vorticity  
1171 patterns in Mediterranean “hurricanes”. *Geophysical Research Letters*, **44** (5), 2537–2545, doi:  
1172 10.1002/2017GL072670.

1173 Min, S.-K., Y.-H. Kim, M.-K. Kim, and C. Park, 2014: Assessing human contribution to the  
1174 summer 2013 Korean heat wave. *Bulletin of the American Meteorological Society*, **95** (9), S48–  
1175 S51.

1176 Miralles, D. G., A. J. Teuling, C. C. van Heerwaarden, and J. V.-G. de Arellano, 2014: Mega-  
1177 heatwave temperatures due to combined soil desiccation and atmospheric heat accumulation.  
1178 *Nature Geoscience*, **7** (5), 345–349.

1179 Mohr, K. I., and E. J. Zipser, 1996: Mesoscale convective systems defined by their 85-ghz  
1180 ice scattering signature: Size and intensity comparison over tropical oceans and continents.  
1181 *Monthly Weather Review*, **124** (11), 2417 – 2437, doi:10.1175/1520-0493(1996)124<2417:  
1182 MCSDBT>2.0.CO;2.

1183 Monhart, S., C. Spirig, J. Bhend, K. Bogner, C. Schär, and M. A. Liniger, 2018: Skill of Sub-  
1184 seasonal Forecasts in Europe: Effect of Bias Correction and Downscaling Using Surface Ob-

1185 servations. *J. Geophys. Res. Atmos.*, doi:10.1029/2017JD027923, URL <http://doi.wiley.com/10.1029/2017JD027923>.

1187 Muñoz, Á. G., 2020: PyCPT: A Python interface and enhancement for IRI's Climate Predictability  
1188 Tool. Tech. rep. doi:10.5281/zenodo.3551936.

1189 Muñoz, Á. G., and Coauthors, 2019: NextGen: A Next-Generation System for Calibrating,  
1190 Ensembling and Verifying Regional Seasonal and Subseasonal Forecasts. *American Geophysical  
1191 Union, Fall Meeting December 2019, abstract #A23U-3024.*

1192 Muñoz, Á. G., L. Goddard, S. J. Mason, and A. W. Robertson, 2016: Cross-time scale interactions  
1193 and rainfall extreme events in southeastern South America for the austral summer. Part II:  
1194 Predictive skill. *Journal of Climate*, **29** (16), 5915–5934, doi:10.1175/JCLI-D-15-0699.1.

1195 Muñoz, Á. G., L. Goddard, A. W. Robertson, Y. Kushnir, and W. Baethgen, 2015: Cross-time  
1196 scale interactions and rainfall extreme events in southeastern South America for the austral  
1197 summer. Part I: Potential predictors. *Journal of Climate*, **28** (19), 7894–7913, doi:10.1175/  
1198 JCLI-D-14-00693.1.

1199 Mueller, B., and S. I. Seneviratne, 2012: Hot days induced by precipitation deficits at the global  
1200 scale. *Proceedings of the National Academy of Sciences of the United States of America*, **109** (31),  
1201 12 398–12 403.

1202 Mylonas, M. P., P. T. Nastos, and I. T. Matsangouras, 2018: PBL parameterization schemes  
1203 sensitivity analysis on WRF modeling of a tornadic event environment in Skala Lakonia in  
1204 September 2015. *Atmospheric Research*, **208**, 116–131, doi:10.1016/j.atmosres.2017.11.023,  
1205 URL <https://linkinghub.elsevier.com/retrieve/pii/S0169809517306099>.

1206 Nicholls, N., 1979: A possible method for predicting seasonal tropical cyclone activity in the  
1207 Australian region. *Mon. Wea. Rev.*, **107**, 1221–1224.

1208 NOAA, 2018: Assessing the U.S. Climate in July 2018. URL <https://www.ncei.noaa.gov/news/national-climate-201807>.

1210 Noer, G., Ø. Saetra, T. Lien, and Y. Gusdal, 2011: A climatological study of polar lows in the  
1211 nordic seas. *Quarterly Journal of the Royal Meteorological Society*, **137 (660)**, 1762–1772.

1212 Pan, B., K. Hsu, A. AghaKouchak, S. Sorooshian, and W. Higgins, 2019: Precipitation prediction  
1213 skill for the West Coast United States: From short to extended range. *Journal of Climate*, **32**,  
1214 161–182.

1215 Pepler, A. S., L. B. Díaz, C. Prodhomme, F. J. Doblas-Reyes, and A. Kumar, 2015: The ability of  
1216 a multi-model seasonal forecasting ensemble to forecast the frequency of warm, cold and wet  
1217 extremes. *Weather and Climate Extremes*, **9**, 68–77.

1218 Perez-Zanon, N., and Coauthors, 2019: *CSTools: Assessing Skill of Climate Forecasts on Seasonal-*  
1219 *to-Decadal Timescales*. URL <http://CRAN.R-project.org/package=CSTools>, r package version  
1220 2.0.0.

1221 Perkins, S., L. Alexander, and J. Nairn, 2012: Increasing frequency, intensity and duration of  
1222 observed global heatwaves and warm spells. *Geophysical Research Letters*, **39 (20)**.

1223 Pfahl, S., and H. Wernli, 2012: Quantifying the relevance of atmospheric blocking for co-located  
1224 temperature extremes in the Northern Hemisphere on (sub-)daily time scales. *Geophysical*  
1225 *Research Letters*, **39 (12)**.

1226 Pineda, L., J. Changoluisa, and A. Muñoz, 2021: Heavy rainfall in the northern coast of Ecuador  
1227 in the aftermath of El Niño 2015/2016 and its predictability. *EGU General Assembly*, **(EGU21-**  
1228 **8559)**, doi:10.5194/egusphere-egu21-8559.

1229 Portmann, R., J. J. González-Alemán, M. Sprenger, and H. Wernli, 2019: Medicane Zorbas:  
1230 Origin and impact of an uncertain potential vorticity streamer. *Weather and Climate Dynamics*  
1231 *Discussions*, 1–30.

1232 Prein, A. F., R. M. Rasmussen, K. Ikeda, C. Liu, M. P. Clark, and G. J. Holland, 2017: The future  
1233 intensification of hourly precipitation extremes. *Nature Climate Change*, **7 (1)**, 48–52.

1234 Prior, J., and M. Kendon, 2011: The disruptive snowfalls and very low temperatures of late 2010.  
1235 *Weather*, **66 (12)**, 315–321.

1236 Program, G. V., 2018: Report on Volcán de Fuego, Guatemala. Tech. rep. doi:10.5479/si.GVP.  
1237 BGVN201808-342090.

1238 Quinting, J. F., and F. Vitart, 2019: Representation of Synoptic-Scale Rossby Wave Packets  
1239 and Blocking in the S2S Prediction Project Database. *Geophysical Research Letters*, **46 (2)**,  
1240 1070–1078.

1241 R Core Team, 2015: *R: A Language and Environment for Statistical Computing*. Vienna, Austria,  
1242 R Foundation for Statistical Computing, URL <http://www.R-project.org/>.

1243 Rasmussen, E., 1983: A review of meso-scale disturbances in cold air masses. *Mesoscale meteo-*  
1244 *rology—theories, observations and models*, 247–283.

1245 Raymond, C., T. Matthews, and R. M. Horton, 2020: The emergence of heat and humidity too  
1246 severe for human tolerance. *Science advances*, **6 (19)**, eaaw1838.

1247 Risbey, J. S., and Coauthors, 2021: Standard assessments of climate forecast skill can be misleading.

1248 *Nature Communications*, **12** (1), 4346–14.

1249 Robertson, A. W., F. Vitart, and S. J. Camargo, 2020: Sub-seasonal to seasonal prediction of

1250 weather to climate with application to tropical cyclones. *J. Geophys. Res.*, **125**, e2018JD029 375,

1251 doi:10.1029/2018JD029375.

1252 Rodney, M., H. Lin, and J. Derome, 2013: Subseasonal Prediction of Wintertime North American

1253 Surface Air Temperature during Strong MJO Events. *Monthly Weather Review*, **141** (8), 2897–

1254 2909.

1255 RTE, 2017: Aperçu mensuel sur l'énergie électrique. Tech. rep. URL <https://assets.rte-france.com/>

1256 prod/public/2020-06/apercu\_energie\_elec\_2017\_01.pdf.

1257 Russo, S., and Coauthors, 2014: Magnitude of extreme heat waves in present climate and their

1258 projection in a warming world. *Journal of Geophysical Research: Atmospheres*, **119** (22),

1259 12–500.

1260 Schaller, N., J. Sillmann, J. Anstey, E. M. Fischer, C. M. Grams, and S. Russo, 2018: Influence

1261 of blocking on Northern European and Western Russian heatwaves in large climate model

1262 ensembles. *Environmental Research Letters*, **13** (5), 054 015.

1263 Seneviratne, S. I., T. Corti, E. L. Davin, M. Hirschi, E. B. Jaeger, I. Lehner, B. Orlowsky, and A. J.

1264 Teuling, 2010: Investigating soil moisture–climate interactions in a changing climate: A review.

1265 *Earth Science Reviews*, **99** (3-4), 125–161.

1266 Service, H. N. M., 2019: Significant weather and climate events in Greece 2018. URL [http://www.hnms.gr/emy/en/pdf/2018\\_GRsignificantEVENT\\_en.pdf](http://www.hnms.gr/emy/en/pdf/2018_GRsignificantEVENT_en.pdf), 12 pp.

1267

1268 Shiogama, H., M. Watanabe, Y. Imada, M. Mori, Y. Kamae, M. Ishii, and M. Kimoto, 2014:  
1269 Attribution of the June-July 2013 heat wave in the southwestern United States. *SOLA*, **10**,  
1270 122–126.

1271 Sinclair, V. A., J. W. Mikkola, M. Rantanen, and J. Räisänen, 2019: The summer 2018 heatwave  
1272 in Finland. *Weather*, **74** (11).

1273 Specq, D., L. Batté, M. Déqué, and C. Ardilouze, 2020: Multimodel Forecasting of Precipitation  
1274 at Subseasonal Timescales Over the Southwest Tropical Pacific. *Earth and Space Science*, **7** (9),  
1275 e2019EA001 003.

1276 Stocker, T., 2014: *Climate change 2013: the physical science basis: Working Group I con-*  
1277 *tribution to the Fifth assessment report of the Intergovernmental Panel on Climate Change.*  
1278 Cambridge university press, Cambridge, United Kingdom and New York, NY, USA, doi:  
1279 10.1017/CBO9781107415324.

1280 Sun, L., C. Deser, and R. A. Tomas, 2015: Mechanisms of Stratospheric and Tropospheric  
1281 Circulation Response to Projected Arctic Sea Ice Loss\*. *Journal of Climate*, **28**, 7824–7845.

1282 Sun, Y., X. Zhang, F. W. Zwiers, L. Song, H. Wan, T. Hu, H. Yin, and G. Ren, 2014: Rapid  
1283 increase in the risk of extreme summer heat in Eastern China. *Nature Climate Change*, **4** (12),  
1284 1082–1085.

1285 Thompson, D., M. Baldwin, and J. Wallace, 2002: Stratospheric connection to Northern Hemi-  
1286 sphere wintertime weather: Implications for prediction. *J. Clim.*, **15**, 1421–1428.

1287 Tian, D., M. Pan, L. Jia, G. Vecchi, and E. F. Wood, 2016: Assessing GFDL high-resolution climate  
1288 model water and energy budgets from AMIP simulations over Africa. *Journal of Geophysical*  
1289 *Research-Atmospheres*, **121** (14), 8444–8459.

1290 Tian, D., M. Pan, and E. F. Wood, 2018: Assessment of a High-Resolution Climate Model  
1291 for Surface Water and Energy Flux Simulations over Global Land: An Intercomparison with  
1292 Reanalyses. *Journal of Hydrometeorology*, **19** (7), 1115–1129.

1293 Tian, D., E. F. Wood, and X. Yuan, 2017: CFSv2-based sub-seasonal precipitation and temperature  
1294 forecast skill over the contiguous United States. *Hydrology and Earth System Sciences*, **21** (3),  
1295 1477–1490.

1296 Tippett, M. K., T. DelSole, S. J. Mason, and A. G. Barnston, 2008: Regression-Based Methods for  
1297 Finding Coupled Patterns. *Journal of Climate*, **21** (17), 4384–4398.

1298 Torralba, V., F. J. Doblas-Reyes, D. MacLeod, I. Christel, and M. Davis, 2017: Seasonal Climate  
1299 Prediction: A New Source of Information for the Management of Wind Energy Resources.  
1300 *J. Appl. Meteorol. Climatol.*, **56** (5), 1231–1247, doi:10.1175/JAMC-D-16-0204.1, URL <http://journals.ametsoc.org/doi/10.1175/JAMC-D-16-0204.1>.

1301 Ulbrich, U., G. C. Leckebusch, and J. G. Pinto, 2009: Extra-tropical cyclones in the present and  
1302 future climate: a review. *Theoretical and Applied Climatology*, **96** (1), 117–131.

1303 Vigaud, N., A. W. Robertson, and M. K. Tippett, 2017: Multimodel Ensembling of Subseasonal  
1304 Precipitation Forecasts over North America. *Monthly Weather Review*, **145** (10), 3913–3928.

1305 Vitart, F., 2014: Evolution of ECMWF sub-seasonal forecast skill scores. *Quarterly Journal of the  
1306 Royal Meteorological Society*, **140** (683), 1889–1899.

1307 Vitart, F., 2017: Madden-Julian Oscillation prediction and teleconnections in the S2S. *Q. J. Roy.  
1308 Meteorol. Soc.*, **143**, 2210–2220, doi:10.1002/qj3079.

1309 Vitart, F., D. Anderson, and T. Stockdale, 2003: Seasonal forecasting of tropical cyclone landfall  
1310 over Mozambique. *J. Climate*, **16**, 3932–3945.

1312 Vitart, F., J. L. Anderson, and W. F. Stern, 1997: Simulation of interannual variability of tropical  
1313 storm frequency in an ensemble of GCM integrations. *J. Climate*, **10**, 745–760.

1314 Vitart, F., A. Leroy, and M. C. Wheeler, 2010: A comparison of dynamical and statistical predictions  
1315 of weekly tropical cyclone activity in the southern hemisphere. *Mon. Wea. Rev.*, **138**, 3671–3682.

1316 Vitart, F., and F. Molteni, 2010: Simulation of the Madden– Julian Oscillation and its teleconnec-  
1317 tions in the ECMWF forecast system. *Quarterly Journal of the Royal Meteorological Society*,  
1318 **136 (649)**, 842–855.

1319 Vitart, F., and A. W. Robertson, 2018: The sub-seasonal to seasonal prediction project (S2S) and  
1320 the prediction of extreme events. *npj Clim. Atmos. Sci.*, **1**, 3, doi:10.1038/s41612-018-0013-0.

1321 Vitart, F., and Coauthors, 2008: The new VarEPS-monthly forecasting system: A first step towards  
1322 seamless prediction. *Quarterly Journal of the Royal Meteorological Society*, **134 (636)**, 1789–  
1323 1799, doi:10.1002/qj.322.

1324 Vitart, F., and Coauthors, 2017: The Subseasonal to Seasonal (S2S) Prediction Project  
1325 Database. *Bulletin of the American Meteorological Society*, **98 (1)**, 163–173, doi:10.1175/  
1326 BAMS-D-16-0017.1.

1327 Vitart, F., and Coauthors, 2019: Chapter 17 - Sub-seasonal to Seasonal Prediction of Weather  
1328 Extremes. *Sub-Seasonal to Seasonal Prediction*, A. W. Robertson, and F. Vitart, Eds., Elsevier,  
1329 365–386, doi:10.1016/B978-0-12-811714-9.00017-6.

1330 Wang, J., Z. Yan, X.-W. Quan, and J. Feng, 2017: Urban warming in the 2013 summer heat wave  
1331 in eastern China. *Climate Dynamics*, **48 (9-10)**, 3015–3033.

1332 Watanabe, M., H. Shiogama, Y. Imada, M. Mori, M. Ishii, and M. Kimoto, 2013: Event Attribution  
1333 of the August 2010 Russian Heat Wave. *SOLA*, **9**, 65–68, doi:10.2151/sola.2013-015.

1334 Wernli, H., M. Paulat, M. Hagen, and C. Frei, 2008: SAL—A Novel Quality Measure for the  
1335 Verification of Quantitative Precipitation Forecasts. *Monthly Weather Review*, **136** (11), 4470–  
1336 4487.

1337 Westra, S., L. V. Alexander, and F. W. Zwiers, 2013: Global Increasing Trends in Annual Maximum  
1338 Daily Precipitation. *Journal of Climate*, **26** (11), 3904–3918, doi:10.1175/JCLI-D-12-00502.1.

1339 Wheeler, M. C., and H. H. Hendon, 2004: An All-Season Real-Time Multivariate MJO Index:  
1340 Development of an Index for Monitoring and Prediction. *Monthly Weather Review*, **132** (8),  
1341 1917–1932.

1342 White, C. J., and Coauthors, 2017: Potential applications of subseasonal-to-seasonal (S2S) pre-  
1343 dictions. *Meteorological Applications*, **24** (3), 315–325.

1344 White, C. J., and Coauthors, 2021: Advances in the application and utility of subseasonal-to-  
1345 seasonal predictions. *Bull. Amer. Meteor. Soc.*

1346 Wilks, D. S., 2019: *Statistical Methods in the Atmospheric Sciences*. 4th ed., Elsevier/Academic  
1347 Press, 840 pp.

1348 Wirth, V., M. Riemer, E. K. M. Chang, and O. Martius, 2018: Rossby Wave Packets on the  
1349 Midlatitude Waveguide—A Review. *Monthly Weather Review*, **146** (7), 1965–2001.

1350 WMO, 2020: Guidance on Operational Practices for Objective Seasonal Forecasting. World Mete-  
1351 orological Organization Commission for Climatology (CCI) and Commission for Basic Systems  
1352 (CBS). Tech. rep., 106 pp. URL [https://library.wmo.int/doc\\_num.php?explnum\\_id=10314](https://library.wmo.int/doc_num.php?explnum_id=10314).

1353 WorldBank, 2018: Concatenated Volcanic Hazards Fuego Volcano crisis. Tech.  
1354 rep. URL <http://documents.worldbank.org/curated/en/360901560919670273/pdf/Concatenated-Volcanic-Hazards-Fuego-Volcano-Crisis.pdf>. Downloaded on April 1st, 2020.

1356 Wu, B., T. Zhou, and T. Li, 2016: Impacts of the Pacific–Japan and circumglobal teleconnection  
1357 patterns on the interdecadal variability of the East Asian summer monsoon. *Journal of Climate*,  
1358 **29** (9), 3253–3271.

1359 Wulff, C. O., and D. I. V. Domeisen, 2019: Higher Subseasonal Predictability of Extreme Hot  
1360 European Summer Temperatures as Compared to Average Summers. *Geophysical Research  
1361 Letters*, **46** (20), 11 520–11 529.

1362 Wulff, C. O., R. J. Greatbatch, D. I. V. Domeisen, G. Gollan, and F. Hansen, 2017: Tropical  
1363 Forcing of the Summer East Atlantic Pattern. *Geophysical Research Letters*, **115** (8), 1083–8.

1364 Yang, J., and Coauthors, 2019: Heatwave and mortality in 31 major Chinese cities: definition,  
1365 vulnerability and implications. *Science of The Total Environment*, **649**, 695–702.

1366 Yasui, S., and M. Watanabe, 2010: Forcing Processes of the Summertime Circumglobal  
1367 Teleconnection Pattern in a Dry AGCM. *Journal of Climate*, **23** (8), 2093–2114, doi:  
1368 10.1175/2009JCLI3323.1.

1369 Yeo, S.-R., S.-W. Yeh, and W.-S. Lee, 2019: Two types of heat wave in Korea associated with  
1370 atmospheric circulation pattern. *Journal of Geophysical Research: Atmospheres*, **124** (14),  
1371 7498–7511.

1372 Yiou, P., and Coauthors, 2019: Analyses of the northern European summer heatwave of 2018.  
1373 *Special Supplement to the Bulletin of the American Meteorological Society*, **101** (1).

1374 Zhang, W., and T. Zhou, 2019: Significant Increases in Extreme Precipitation and the Associations  
1375 with Global Warming over the Global Land Monsoon Regions. *Journal of Climate*, **32** (24),  
1376 8465–8488.

<sub>1377</sub> Zhang, X., H. Wan, F. W. Zwiers, G. C. Hegerl, and S.-K. Min, 2013: Attributing intensification of  
<sub>1378</sub> precipitation extremes to human influence. *Geophysical Research Letters*, **40** (19), 5252–5257,  
<sub>1379</sub> doi:10.1002/grl.51010.

<sub>1380</sub> Zscheischler, J., and Coauthors, 2020: A typology of compound weather and climate events. *Nature  
Reviews Earth & Environment*, **1** (7), 333–347, doi:10.1038/s43017-020-0060-z.  
<sub>1381</sub>

1382 LIST OF TABLES

TABLE 1. Overview of the case studies evaluated in this study.

Location / target region	Forecast target period
<b>HEATWAVES</b>	
Western U.S. (California) (235 - 250°E, 32 - 48°N)	23-29 July 2018
Central / northeastern Europe (10 - 20°E, 50 - 60°N)	23-29 July 2018
Southeastern U.S. (92 - 70°W, 25 - 45°N)	24-30 May 2019
East Asia (eastern China, Korea, Japan) (105 - 130.5°E, 30 - 40.5°N)	5-11 August 2013
<b>COLD SPELLS</b>	
Southeastern Europe (10.5 - 30°E, 37.5 - 54°N)	3-9 April 2003
Central / northern Europe (12.5°W - 30°E, 37.5 - 65°N)	26 February - 3 March 2018
Southwestern Europe (France) (4.5°W - 7.5°E, 43.5 - 49.5°N)	16-22 January 2017
Northern Europe (UK, Germany, Scandinavia) (10°W - 30°E, 45 - 65°N)	27 November - 3 December 2010
<b>PRECIPITATION EVENTS</b>	
Volcán de Fuego, Guatemala (91 °W, 14.5 °N)	18-24 June 2018
Northwestern Ecuador (79 °W, 0 °N)	21-27 January 2016
Northwestern Italy (6.5 - 10°E, 43.5 - 46.5°N)	21-27 November 2016
Northeastern Australia (138°-147°E, 18°-22°S)	31 January - 6 February 2019
<b>CYCLOCNES</b>	
Western Australia: Cyclone Claudia (no landfall)	5 January 2020 (formation) / 18 January 2020 (dissipation)
Mozambique Channel: Cyclone Belna (landfall: Madagascar)	2 December 2019 (formation) / 9 December 2019 (landfall)
Western North Pacific: Typhoon Chan-hom (landfall: China)	29 June 2015 (formation) / 11 July 2015 (landfall)
Mediterranean: Medicane Zorbas (landfall: Peloponnese, Greece)	27 September 2018 (formation) / 29 September 2018 (landfall)

## LIST OF FIGURES

1385 **Fig. 1.** **Heatwaves:** (a,c,e,g) 2m temperature anomalies for the target week (indicated in the panel  
 1386 titles) from ERA5 data and (b,d,f,h) predicted by the ECMWF week 3 forecasts (hindcasts  
 1387 prior to 2016), initialization dates indicated in panel titles. (a,b) California heatwave, (c,d)  
 1388 European heatwave, (e,f) U.S. heatwave, (g,h) East Asia heatwave. White boxes indicate the  
 1389 averaging areas used for Fig. 2. All case studies use model version CY45R1, except for the  
 1390 East Asia heatwave, which uses CY46R1. . . . .

1391 **Fig. 2.** **Heatwaves:** The PDF distribution of the predicted 2m temperature anomalies from the model  
 1392 ensemble averaged over the target week (indicated in table 1) for the heatwave case studies,  
 1393 averaged over the white boxes in Fig. 1 and initialized at (panels from left to right) 4, 3, and  
 1394 2 weeks before the start of the target week. (a) California heat wave 2018, (b) European heat  
 1395 wave 2018, (c) southeastern U.S. heat wave 2019, and (d) east Asia heatwave 2013. Tercile  
 1396 limits (below-normal: blue, normal: gray, and above-normal: red) are computed with respect  
 1397 to the lead time - dependent model climatology. Values above the 66th percentile (below  
 1398 the 33rd percentile) are represented by red (blue) shading. Grey shading represents values  
 1399 between these terciles. The yellow dots indicate the ensemble members that were used to  
 1400 construct the PDF (51 for forecasts, 11 for hindcasts) . . . . . 68

1401 **Fig. 3.** **Cold spells:** Same as Figure 1 but for the cold spell case studies: (a,b) Southeastern Europe  
 1402 cold spell in 2003 (model version CY46R1), (c,d) central / northern European cold spell in  
 1403 2018 (model version CY43R3), (e,f) France cold spell in 2017 (model version CY43R1),  
 1404 (g,h) northern European cold spell in 2010 (model version CY46R1). . . . . 69

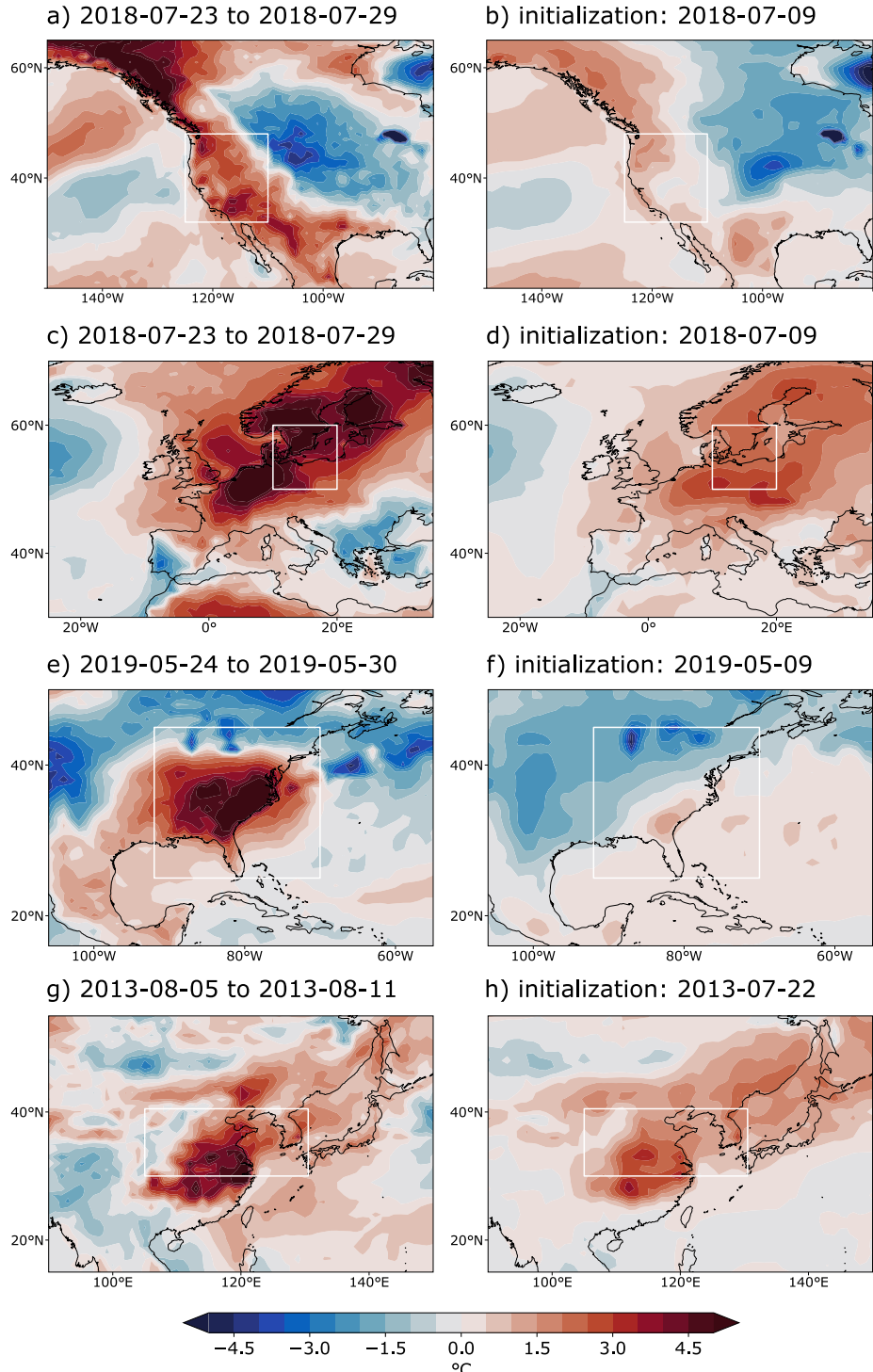
1405 **Fig. 4.** **Cold spells:** Same as Figure 2 but for the cold spell case studies: (a) Southeastern Europe  
 1406 cold spell in 2003, (b) European cold spell in 2018, (c) France cold spell in 2017, and (d) the  
 1407 northern European cold spell in 2010. . . . . 70

1408 **Fig. 5.** **Precipitation events:** Accumulated precipitation anomalies over the target week (week 3,  
 1409 indicated in the panel titles) for (a,c,e,g) observations and (b,d,f,h) the ECMWF model prediction  
 1410 (initialization date indicated in the panel title). (a,b) Guatemala, (c,d) western Ecuador  
 1411 (e,f) northwestern Italy, and (g,h) northeastern Australia. The blue boxes or dots, respec-  
 1412 tively, indicate the target location for each case study, as indicated in Table 1. Observations  
 1413 are from (a,c,e) CPC and (g) AWAP. . . . . 71

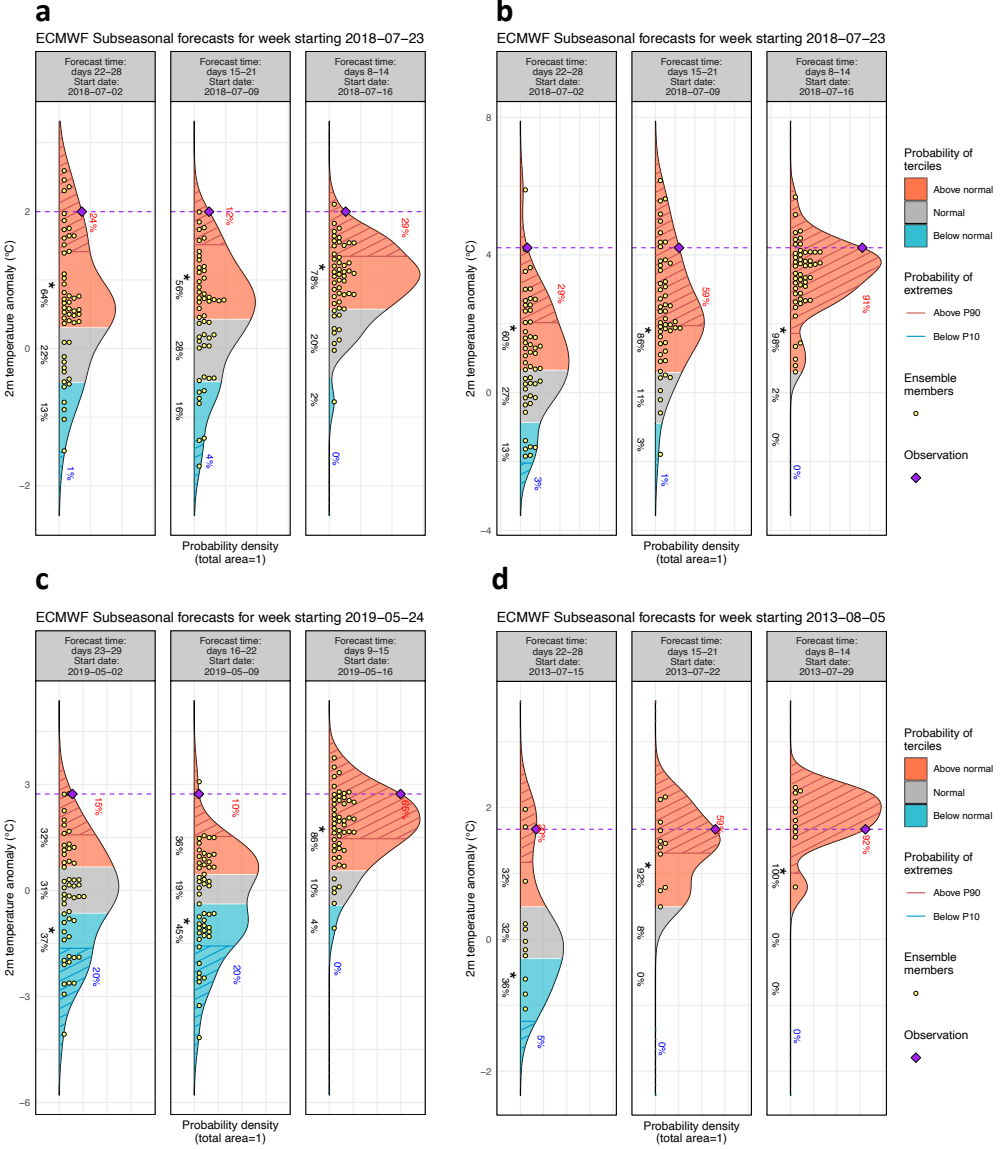
1414 **Fig. 6.** **Precipitation extremes:** Predictability scores for week 3, (a,c,e,g) assessed through the  
 1415 area under the ROC curve for the above-normal category, and (b,d,f,h) Spearman's rank  
 1416 correlation coefficient. The results were interpolated to the CPC unified grid. For details  
 1417 of the scores see section 2. (a,b) Guatemala, (c,d) western Ecuador (e,f) northwestern Italy,  
 1418 and (g,h) northeastern Australia. The blue boxes or dots are as in Figure 5. . . . . 72

1419 **Fig. 7.** **Cyclones:** Satellite images at a time close to the maximum intensity of the storms for (a) cy-  
 1420 clone Claudia on January 13, 2020 [NOAA] (c) cyclone Belna on December 7, 2019 [NASA],  
 1421 (e) typhoon Chan-hom on July 10, 2015 [SSEC/CIMSS, University of Wisconsin–Madison],  
 1422 and (g) medicane Zorbas (2018M02) on September 29, 2018 [MODIS NASA]. (b,d,f,h)  
 1423 Probability of cyclone occurrence for (b) Claudia initialized on 30/12/2019 for lead times of  
 1424 15–21 days, (d) Belna initialized on 18/11/2019 for lead times of 22–28 days, (f) Chan-hom  
 1425 initialized on 15/06/2015 for lead times of 22–28 days, and (h) medicane Zorbas initialized  
 1426 on 13/09/2018 for lead times of 0–32 days. Black lines indicate the observed cyclone tracks  
 1427 during the verification period, and the names of the cyclones corresponding to the tracks are  
 1428 indicated. The different choice of lead times for the case studies refers to the furthest lead  
 1429 time for which the events were possible to be predicted. . . . . 73

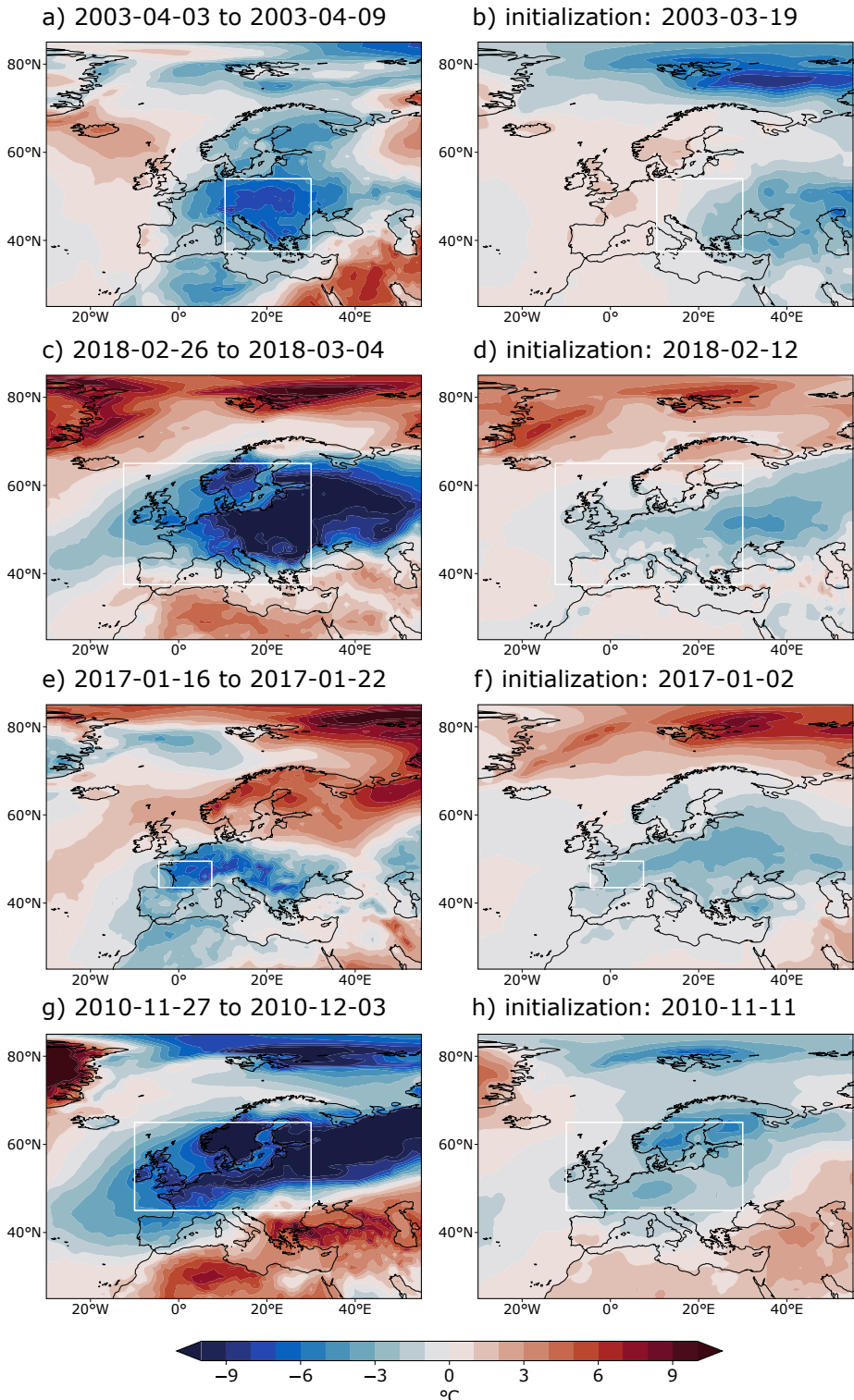
**Fig. 8.** **Cyclones:** Outgoing longwave radiation (OLR) anomalies (shaded,  $\text{W m}^{-2}$ ) and MJO-filtered OLR anomalies (red contours, every 15  $\text{W m}^{-2}$  for negative values) from (a,c) observations averaged over 0-10°N and 0-10°S with tropical cyclone tracks (black lines) and names (first letter of the cyclone name in red circle) and (b,d) ECMWF ensemble forecasts initialized on 15/06/2015 and 18/11/2019. MJO-filtering is performed using a wavenumber-frequency filter that selects for wavenumbers 0-9 and periods of 20-100 days. MJO-filtered OLR was calculated by padding the forecast with observations prior to initialization following the methodology described in Janiga et al. (2018). (e) CAPE ( $\text{J kg}^{-1}$ ) from the ECMWF ensemble forecast initialized on 30/08/2018, valid on 26/09/2018.



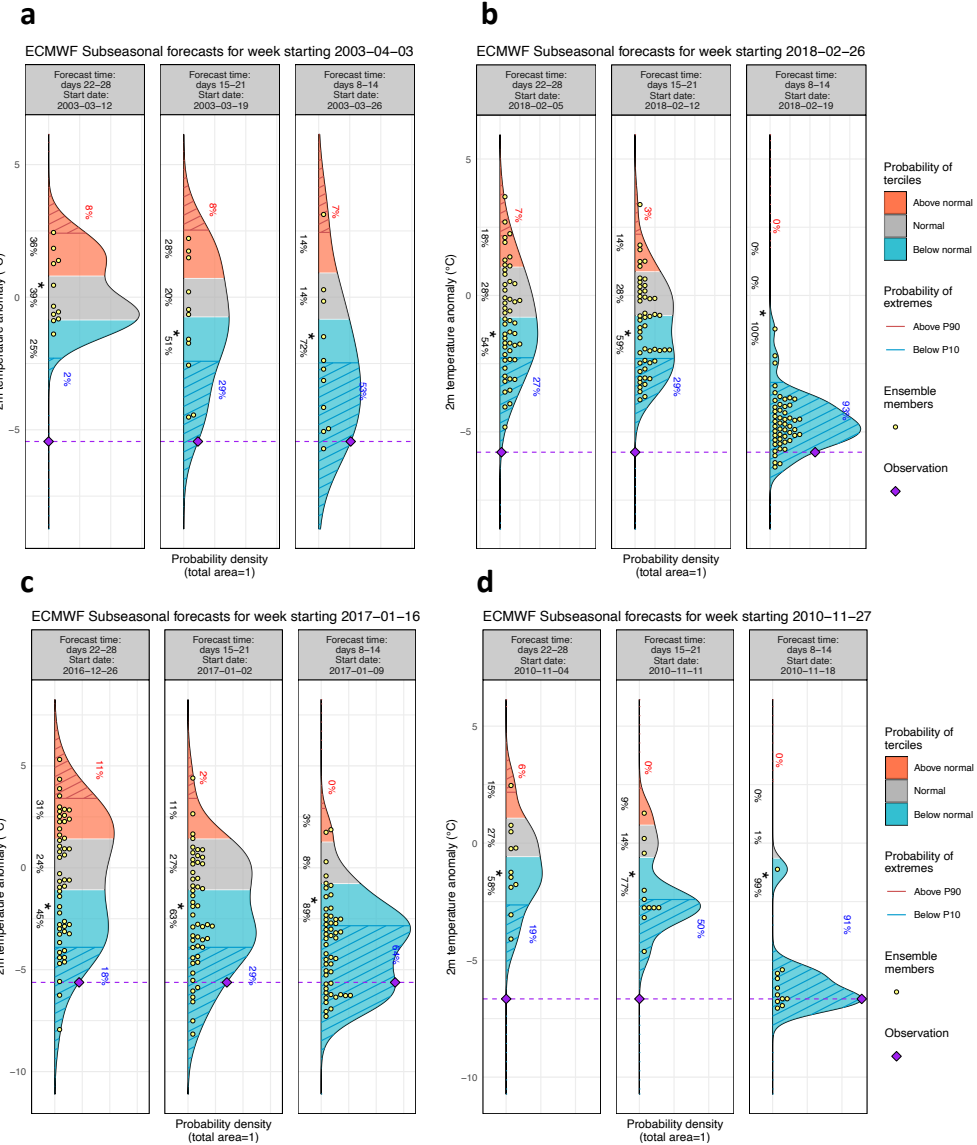
1439 **FIG. 1. Heatwaves:** (a,c,e,g) 2m temperature anomalies for the target week (indicated in the panel titles) from  
 1440 ERA5 data and (b,d,f,h) predicted by the ECMWF week 3 forecasts (hindcasts prior to 2016), initialization dates  
 1441 indicated in panel titles. (a,b) California heatwave, (c,d) European heatwave, (e,f) U.S. heatwave, (g,h) East Asia  
 1442 heatwave. White boxes indicate the averaging areas used for Fig. 2. All case studies use model version CY45R1,  
 1443 except for the East Asia heatwave, which uses CY46R1  
 69



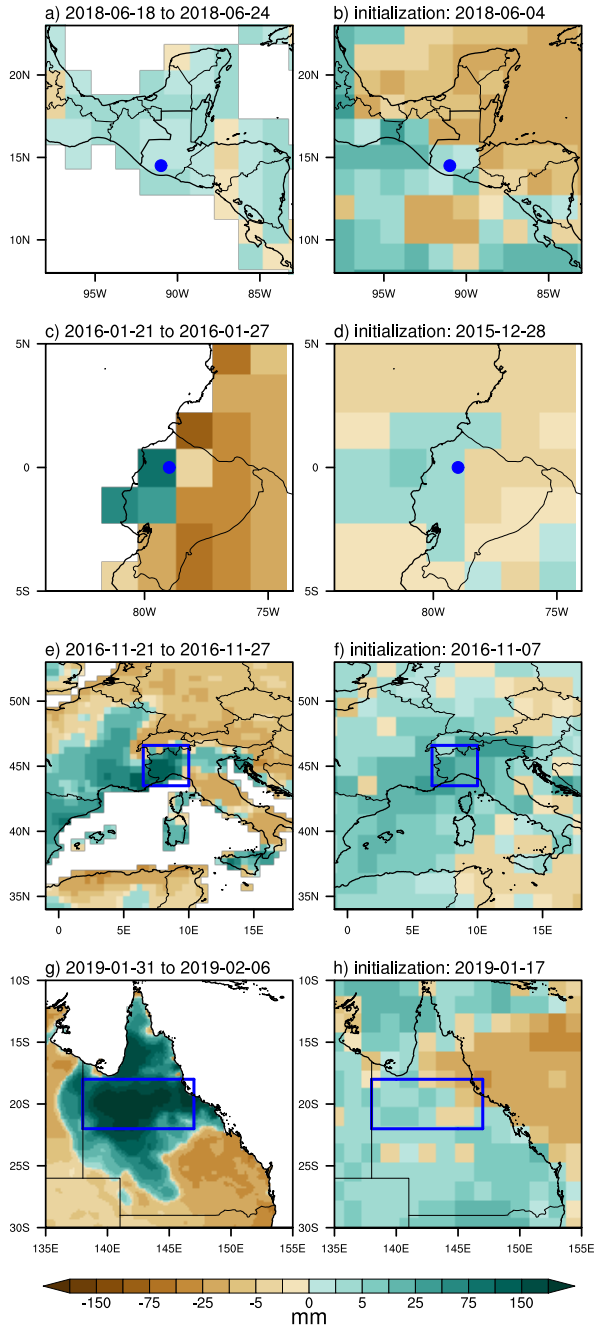
1444 **FIG. 2. Heatwaves:** The PDF distribution of the predicted 2m temperature anomalies from the model ensemble  
 1445 averaged over the target week (indicated in table 1) for the heatwave case studies, averaged over the white boxes  
 1446 in Fig. 1 and initialized at (panels from left to right) 4, 3, and 2 weeks before the start of the target week. (a)  
 1447 California heat wave 2018, (b) European heat wave 2018, (c) southeastern U.S. heat wave 2019, and (d) east  
 1448 Asia heatwave 2013. Tercile limits (below-normal: blue, normal: gray, and above-normal: red) are computed  
 1449 with respect to the lead time - dependent model climatology. Values above the 66th percentile (below the 33rd  
 1450 percentile) are represented by red (blue) shading. Grey shading represents values between these terciles. The  
 1451 yellow dots indicate the ensemble members that were used to construct the PDF (51 for forecasts, 11 for hindcasts)  
 . The extremes above the 90th (below the 10th) percentile are hatched and their probabilities are  
 indicated by red (blue) numbers, respectively. The purple dashed line represents the anomaly in  
 ERA5 reanalysis averaged over the target week.



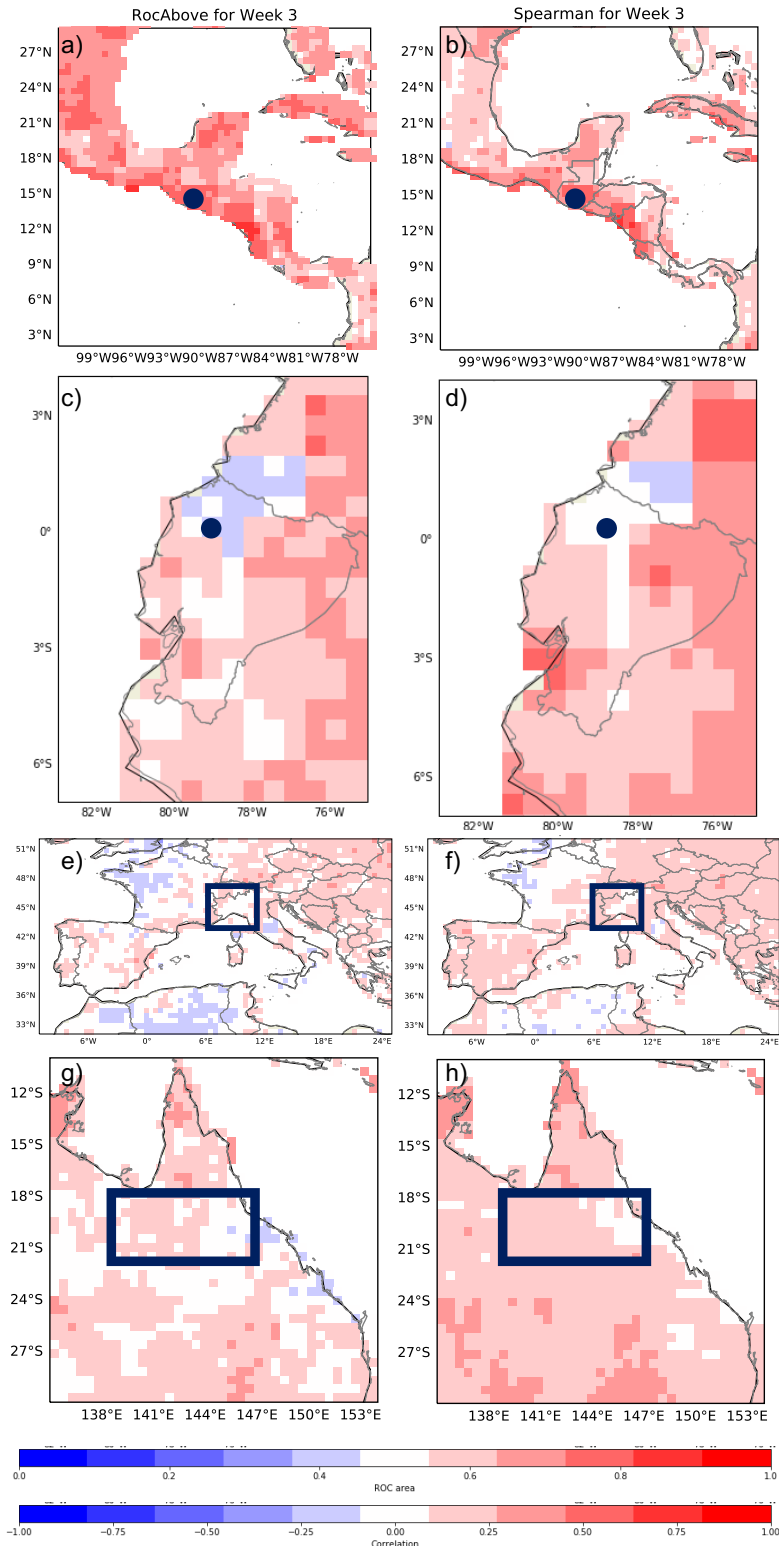
1452 **FIG. 3. Cold spells:** Same as Figure 1 but for the cold spell case studies: (a,b) Southeastern Europe cold spell  
 1453 in 2003 (model version CY46R1), (c,d) central / northern European cold spell in 2018 (model version CY43R3),  
 1454 (e,f) France cold spell in 2017 (model version CY43R1), (g,h) northern European cold spell in 2010 (model  
 1455 version CY46R1).



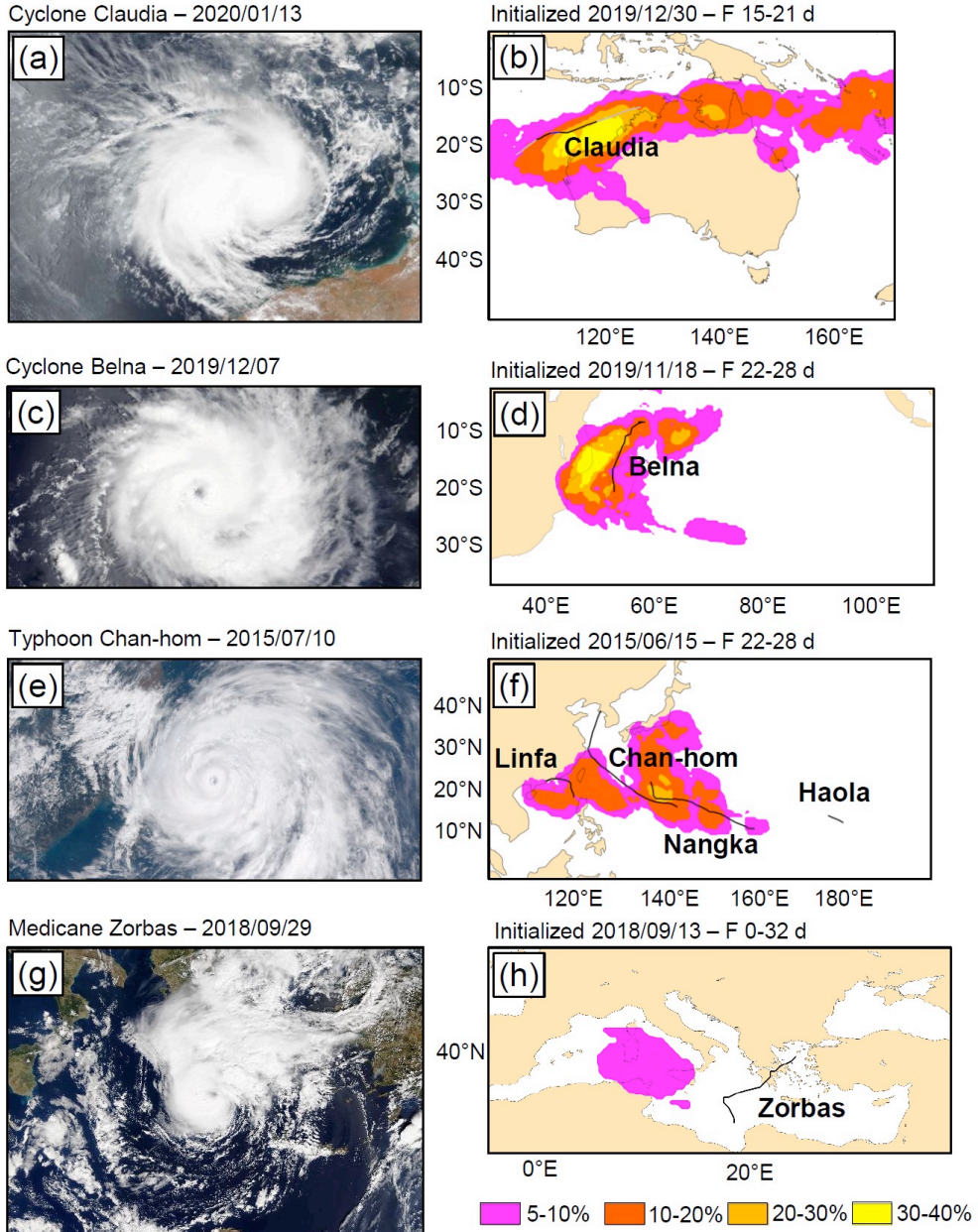
1456 **FIG. 4. Cold spells:** Same as Figure 2 but for the cold spell case studies: (a) Southeastern Europe cold spell  
 1457 in 2003, (b) European cold spell in 2018, (c) France cold spell in 2017, and (d) the northern European cold spell  
 1458 in 2010.



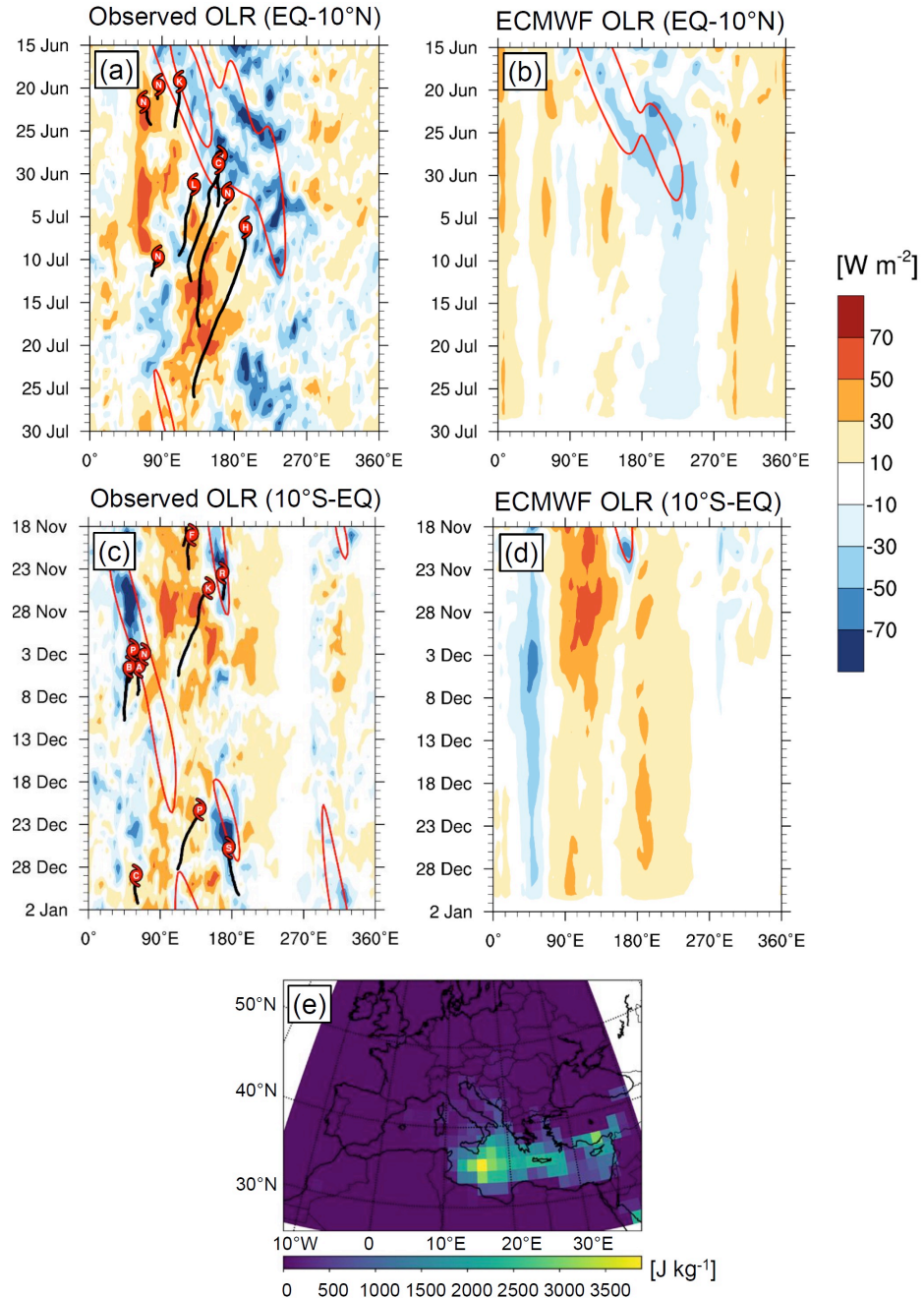
1459 **FIG. 5. Precipitation events:** Accumulated precipitation anomalies over the target week (week 3, indicated in  
 1460 the panel titles) for (a,c,e,g) observations and (b,d,f,h) the ECMWF model prediction (initialization date indicated  
 1461 in the panel title). (a,b) Guatemala, (c,d) western Ecuador (e,f) northwestern Italy, and (g,h) northeastern  
 1462 Australia. The blue boxes or dots, respectively, indicate the target location for each case study, as indicated in  
 1463 Table 1. Observations are from (a,c,e) CPC and (g) AWAP.



1464 **FIG. 6. Precipitation extremes:** Predictability scores for week 3, (a,c,e,g) assessed through the area under  
 1465 the ROC curve for the above-normal category, and (b,d,f,h) Spearman's rank correlation coefficient. The results  
 1466 were interpolated to the CPC unified grid. For details of the scores see section 2. (a,b) Guatemala, (c,d) western  
 1467 (e,f) northwestern Italy, and (g,h) northeastern Australia. The blue boxes or dots are as in Figure 5.  
 74



1468 **FIG. 7. Cyclones:** Satellite images at a time close to the maximum intensity of the storms for (a) cyclone  
 1469 Claudia on January 13, 2020 [NOAA] (c) cyclone Belna on December 7, 2019 [NASA], (e) typhoon Chan-hom  
 1470 on July 10, 2015 [SSEC/CIMSS, University of Wisconsin–Madison], and (g) medicane Zorbas (2018M02) on  
 1471 September 29, 2018 [MODIS NASA]. (b,d,f,h) Probability of cyclone occurrence for (b) Claudia initialized  
 1472 on 30/12/2019 for lead times of 15–21 days, (d) Belna initialized on 18/11/2019 for lead times of 22–28 days,  
 1473 (f) Chan-hom initialized on 15/06/2015 for lead times of 22–28 days, and (h) medicane Zorbas initialized on  
 1474 13/09/2018 for lead times of 0–32 days. Black lines indicate the observed cyclone tracks during the verification  
 1475 period, and the names of the cyclones corresponding to the tracks are indicated. The different choice of lead  
 1476 times for the case studies refers to the furthest lead time for which the events were possible to be predicted.



1477 **FIG. 8. Cyclones:** Outgoing longwave radiation (OLR) anomalies (shaded,  $\text{W m}^{-2}$ ) and MJO-filtered OLR  
 1478 anomalies (red contours, every  $15 \text{ W m}^{-2}$  for negative values) from (a,c) observations averaged over  $0-10^\circ\text{N}$  and  
 1479  $0-10^\circ\text{S}$  with tropical cyclone tracks (black lines) and names (first letter of the cyclone name in red circle) and  
 1480 (b,d) ECMWF ensemble forecasts initialized on 15/06/2015 and 18/11/2019. MJO-filtering is performed using a  
 1481 wavenumber-frequency filter that selects for wavenumbers 0-9 and periods of 20-100 days. MJO-filtered OLR was  
 1482 calculated by padding the forecast with observations prior to initialization following the methodology described  
 1483 in Janiga et al. (2018). (e) CAPE ( $\text{J kg}^{-1}$ ) from the ECMWF ensemble forecast initialized on 30/08/2018, valid  
 1484 on 26/09/2018.